Optimal Smooth Switching of Controllers for Heavy-Duty Vehicles

Master's thesis in Systems, Control and Mechatronics

BASAR ÖZKAN

DEPARTMENT OF ELECTRICAL ENGINEERING

CHALMERS UNIVERSITY OF TECHNOLOGY
Gothenburg, Sweden 2023
www.chalmers.se

Master's thesis 2023

Optimal Smooth Switching of Controllers for Heavy-Duty Vehicles

BASAR ÖZKAN

CHALMERS
UNIVERSITY OF TECHNOLOGY

Department of Electrical Engineering
Division of Systems and Control
Chalmers University of Technology
Gothenburg, Sweden 2023

Optimal Smooth Switching of Controllers for Heavy-Duty Vehicles
BASAR ÖZKAN

Supervisors:
Balázs Adam Kulcsár, Electrical Engineering, Chalmers University of Technology
Björn Viberg, Volvo Group Trucks Technology, Gothenburg, Sweden
Esteban Gelso, Volvo Group Trucks Technology, Gothenburg, Sweden
Maliheh Sadeghi Kati, Volvo Group Trucks Technology, Gothenburg, Sweden
Mats Jonasson, Mechanics and Maritime Sciences, Chalmers University of Technology

Examiner:
Balázs Adam Kulcsár, Electrical Engineering, Chalmers University of Technology

Master's Thesis 2023
Department of Electrical Engineering
Division of Systems and Control
Chalmers University of Technology
SE-412 96 Gothenburg
Telephone +46 31 772 1000

Typeset in LaTeX
Printed by Chalmers Reproservice
Gothenburg, Sweden 2023

Optimal Smooth Switching of Controllers for Heavy-Duty Vehicles
BASAR ÖZKAN
Department of Electrical Engineering
Chalmers University of Technology

Abstract

Heavy road vehicles currently contain different dynamics control systems such as advanced driver assistance control systems (ADAS) and simple rule based control systems. As the transition towards full electrification of heavy vehicles and fully autonomous vehicles continues, newer control systems are being added to current ones. Thus, there is a need to be able to switch between different vehicle control systems. The process of making these types of switches smooth is the topic of this thesis. Smooth switching is considered to occur when there are no large bumps or oscillations during the switching process.

Research done in the area of switching systems usually focuses on having the outputs of the controller coming online to be close to the outputs of the controller going offline so that the transition is smooth. Trying to match the controller outputs does not work for heavy vehicles because of the number of different actuators and the differences in the response rates of these actuators. The contribution of this thesis is to develop and analyze methods of switching between controllers that may have different goals and are acting on differing actuators.

Switching methods of different complexities are developed and analyzed. Preparing the offline controller by connecting it to a model of the real vehicle is shown to decrease the dynamics that occur when the new controller is connected. Using linear interpolation and sigmoid functions to switch from the outputs of the initial controller to the final controller are tested using a realistic simulation environment developed by Volvo Trucks. Filtering these interpolation functions depending on the actuator response rates shows significant decrease in the disturbance to the vehicle during the switching process.

Switching using model predictive control as an in between controller to switch from the tire force forces of the initial controller to the tire forces of the final controller is shown to be feasible. This method has the advantage of achieving optimal switching depending on the priorities of the control designer. Another advantage of the model predictive controller is obtained if the timing of the switch is known before it happens. Using this preview information, the actuators can start changing their outputs even before the switch time for optimal switching performance. Since the model predictive controller requires knowledge of all of the system states a Cubature Kalman filter is developed. This Kalman filter also estimates the tire stiffnesses because it is relatively difficult to know the tire properties of a truck.

Keywords: model predictive control, control allocation, switching systems, bumpless switching, quadratic programming, heavy vehicles.

Acknowledgements

It was a pleasure completing my thesis at Volvo Group Trucks Technology. I would like to thank my supervisors at Volvo GTT, Maliheh Sadeghi Kati, Esteban Gelso and Björn Viberg for their guidance and help during the progression of my thesis. I would like to thank my supervisor, Mats Jonasson from Chalmers University of Technology for interesting discussions which made a strong contribution to my thesis. I would also like to thank my supervisor and examiner Balázs Adam Kulcsár from Chalmers University of Technology for his continuous support, valuable suggestions and constructive feedback.

Finally, I would like to thank my mother, without whose support this thesis would not have been possible.

Basar Özkan, Gothenburg, June 2023

Nomenclature

Below is the nomenclature of acronyms, indices, parameters, and variables that have been used throughout this thesis.

Acronyms

CA	Control Allocation
MPC	Model Predictive Control
VTM	Volvo Truck Model

Indices

i	Index for axle number where i is 1 for front and 2 for rear axle
$trss$	Truck in steady state
mi	i'th electric motor
si	i'th shaft in drive train
ti	i'th tire

Parameters

C_{xi}	Longitudinal slip stiffness coefficient of i'th tire
c_{si}	Stiffness of i'th shaft
d_{si}	Damping of i'th shaft
m_{tr}	Mass of truck
J_{ti}	Rotational moment of inertia of i'th tire
R	Tire radius
g	Gravity constant

τ_e	Time constant of electric motor
τ_b	Time constant of brake actuator
θ_b	Dead time of brake actuator

Variables

v_{tr}	Truck velocity
v_{trss}	Truck velocity in steady state
ω_{mi}	Angular velocity of i'th electric motor
θ_{si}	Twist angle of i'th shaft in drive train
ω_{mi}	Angular velocity of i'th tire
τ_i	Torque of i'th electric motor
F_{ti}	Longitudinal force produced by i'th tire
F_{tiref}	Reference longitudinal force of i'th tire
F_{zi}	Normal force on i'th tire
s_{xi}	Longitudinal slip of i'th tire
C_i	Longitudinal slip stiffness of i'th tire
θ	Road slope angle
T	Sampling time
K_s	Constant for determining slope of sigmoid function
t_d	Time of switch

Contents

List of Figures

1

Introduction

1.1 Background

Heavy road vehicles such as trucks and tractor semi-trailers are an important part of the current transportation system. Improving the safety of these road vehicles has been an area of continuous research in the last several decades. Active control systems have been shown to improve vehicle safety starting with the Anti-lock Braking System (ABS) in 1978 and continued specifically with Electronic Stability Control (ESC) [1]. Currently, there is also a push towards electrification of road vehicles for reaching the goal of sustainable transportation set by the United Nations [2]. Electrification for heavy road vehicles has its own challenges because of the limited energy density of batteries which limits the range of these vehicles [3]. One method of improving the range of heavy road vehicles is using different types of electric motors on different axles of the vehicle. Since different types of electric motors can have different optimal operation properties, the vehicle system can be optimized to use the electric motors in the most efficient proportion [4]. Furthermore, the mechanical brakes have to be used in conjunction with the electric motors. Control Allocation (CA) is a method that can be used in the control of over-actuated systems like the vehicles just described. CA has been used for both stability control [5] and energy optimization [4] in heavy vehicles. There are also older rule-based methods for handling over-actuated heavy vehicles that are currently used in industry.

The number of control systems that exist in heavy vehicles show that there is a need be able to switch between these different control systems. One possible scenario that can occur when using optimization based methods such as CA is that there is no feasible solution to the optimization problem at a certain time instant. This serious problem of having no controller output can be solved by switching to a rule-based method that always produces a control output. This thesis will focus on the issues of switching between different control systems as it relates to heavy vehicles. The goal of this thesis is to develop methods that achieve the switching process smoothly with good performance. Smooth switching is considered to occur when there are no large bumps or oscillations during the switching process. A switching process that has good performance achieves switching in a reasonable amount of time.

1.2 Switching Control Theory Background

1.2.1 Bumpless Transfer

One of the important aspects of switching between controllers is bumpless transfer. This can be thought of from the perspective of switching from an online controller to an offline controller. A bumpless transfer occurs when the output of the offline controller that is coming online is close to the value that is output by the currently online controller [6]. If these values are close there is limited disturbance during the switch. Much research has been done in the area of bumpless transfer using different methods. Studies comparing different methods of bumpless transfer are available [7, 8]. Hard switching is instantly switching between controllers without any consideration of the transients. This method has the advantage of simplicity both in application and also proof of stability. Scaling functions such as sigmoid functions for smoothing transitions between controllers have been applied successfully for vehicle controls problems [9]. However, stability for this type of switching is difficult to prove [8].

Many bumpless transfer methods attach other controllers to the offline controller so that the output of the offline controller tracks the output of the online controller. However, it may not be possible for the offline controller to track the output of the online controller. It has been shown that it is possible to achieve tracking when there are integrators in all of the controller channels and may not be possible if there are no integrators in all of the controller channels [10]. Stability during bumpless transfer is a concern and has been studied by introducing dwell time conditions [11]. Linear quadratic methods have also been shown to be applicable to bumpless transfer. By changing the weights in linear quadratic methods the designer is given the freedom to achieve different signal shapes during the transfer process [12]. The quadratic cost function can be used for several goals such as minimizing control signals, tracking errors and controlled outputs [13]. Switching between different automatic controllers is not the only application of bumpless transfer. Bumpless transfer has also been applied in vehicles when the control of the vehicle is being transferred from the human driver to a driver assist system [14].

1.2.2 Controller Design for Varying Systems

In most controller design procedures a model of the controlled system is used. However, a model of the system is never perfect. Even if a "good" model can be obtained most systems change over time. Control engineers have developed several different methods to solve these issues over the years. Robust control is one of these methods where the uncertainties in the system model and the disturbances are taken into account during the design process [15]. A controller is designed so that the closed loop system is stable and meets performance requirements for all possible cases of system variation. Another method that has been in use for varying systems is gain scheduling. This method is specifically useful in the area of flight control because the aircraft goes through many different flight modes that require different controllers

[16]. The controller gains are varied depending on the flight mode. Adaptive control is the general name for controllers that adapt to changes in the system and gain scheduling is a type of adaptive control [17].

There are different methods for switching between controllers such as Multiple Model Adaptive Control [18] and Iterative Identification Control [17]. In Multiple Model Adaptive Control several models of the system are developed to describe the system under different situations. Furthermore, a controller is designed for each model. A decision making unit decides which model matches the real system the best and chooses the corresponding controller. The Iterative Identification Control method starts off with a basic controller and model. The measurements are used to improve the system model and the controller is updated accordingly. The controller and model are tested offline until the controller is optimized. When the optimized controller is brought online new measurements from obtained from the system and the process is repeated until the controller performance cannot be improved.

1.2.3 Stability of Switching Systems

Stability in a switching system is critical because it is possible to have instability even when switching between two systems that are separately stable [19]. It is also possible to switch between two unstable systems with a switching strategy that makes the overall system stable. However, in vehicle dynamics controls, it is usually the case that the control systems being switched between are stable. Therefore, in this thesis, switching between stable systems is considered. It has been shown that it is more difficult to guarantee arbitrary switching, which is switching at any rate, when compared to slow switching [19]. Therefore, one usually limits the time between switches to prove stability. This time is referred to as dwell time. If dwell time is above a certain value, a linear system can be proven to be stable.

1.3 Purpose

The purpose of this thesis is to develop methods of smooth switching between controllers for heavy vehicles. This purpose is achieved by answering the following research questions with regard to heavy vehicles:

1. What are the possible issues that may occur when switching between different controllers?
2. What methods can be used for switching between different controllers in a smooth manner?
3. Which methods work well for switching when a controller failure occurs and it is necessary to switch to another controller?
4. Which methods work well for switching when the switching time is known beforehand?
5. What are the advantages and disadvantages of different switching strategies?

1.4 Methodology

The steps to achieve the purpose of the thesis are as follows:

1. Research the different methods of switching in the literature.
2. Develop a vehicle model that can be used in the analysis. The model should be simple enough for analysis but still contain realistic dynamics that are present in heavy vehicles.
3. Switch between basic controllers using the detailed vehicle model (VTM) provided by Volvo AB to determine the realistic issues that can occur during the switching process. Conduct these simulations with direct switching methods to understand the problem in detail.
4. Conduct switching between basic controllers with different strategies that are not computationally intensive.
5. Analyze the switching process using the Model Predictive Control method. It should be noted that the goal in this step is not to switch controllers but to develop various MPC based controllers for controlling tire forces to understand the effect of different MPC based controller designs.
6. Develop a state and parameter estimator. The MPC requires knowledge of all states to perform the optimization. Even though these can be measured directly from the model in a simulation environment, in a realistic scenario, the states that cannot be measured must be estimated.
7. Test the switching process between two different controllers using MPC and the basic vehicle model.
8. Test the switching process between two different controllers using MPC and the detailed vehicle model (VTM).
9. Analyze the realistic test case scenario for switching between a CA based controller and a rule based control algorithm using the detailed vehicle model (VTM).

1.5 Scope and Limitations

The scope of the thesis is as follows:

1. The vehicle model used in the controller design consists of the longitudinal vehicle model. Lateral dynamics of the vehicle are not considered.
2. The performance of different switching methods is validated using simulations with a detailed truck model (VTM: Volvo Truck Model) developed by Volvo in the MATLAB/Simulink environment. No experiments are conducted on a real truck.
3. Real time performance of the control algorithms is not considered.
4. Electric motor and braking system models consist of transfer functions and dead time delays which do not take into account all of the detailed dynamics of electric motors and brakes systems.

1.6 Ethical and Sustainability Aspects

The United Nations Sustainability Goals are considered in this thesis. Specifically UN Sustainability Goal 12 concerns responsible consumption and production. Carbon emissions are a leading cause of global warming and must be reduced for sustainable development. Switching to electric vehicles is an important part of reducing carbon emissions and Volvo Trucks is developing electric trucks for this purpose. However, the travel range of these trucks is still limited compared to how much a truck can drive in a day. Different projects at Volvo Trucks are under way to improve the range of these trucks. One method for improvement is to use different electric motors on different axles of the truck and optimize their use for minimum energy consumption [4]. Furthermore, there are other control algorithms for the safe operation of these heavy vehicles. There is a need to switch between these different control algorithms in a smooth and effective manner. This is the main goal of this thesis making it a part of reaching the sustainability goals of the United Nations.

It should be noted that transitioning to electric vehicles in itself does not guarantee decreased carbon emissions because carbon emissions can still be high depending on the method of electricity production. Thus, there is still the risk of not decreasing carbon emissions if the electricity produced in the area that the electric truck is operating is produced with carbon emitting fossil fuels. The recycling of electric truck batteries is also a matter of concern since it concerns toxic materials. This may be an issue in countries where environmental laws are not strict or are not being enforced. In these circumstances the toxic materials can end up in places where they can harm humans or other living organisms.

Developing complicated control algorithms that require many actuators and sensors for the purpose of having very high efficiency can also have negative consequences. The more complicated a system is, the more parts of the system there are that can fail. A failure in a heavy vehicle control system can result in a traffic accident. A traffic accident can cause loss of life or human suffering if someone is hurt. Furthermore, heavy vehicles can carry toxic substances that can spill into the environment in the case of an accident. This could result in pollution of the area and also harm the living organisms in the area. A traffic accident of a heavy vehicle can also cause material damage to the truck, other vehicles and infrastructure.

No individual or personal data is used in this project, the method will aim at executing switching in a smooth and cost efficient way. The method can not be used to discriminate, fairness is by default included (no priority or advantage can be given in the algorithm to discriminate).

Artificial intelligence was not used in the writing of this thesis.

1.7 Thesis Outline

In Chapter 2 a longitudinal vehicle model is developed. This model is used in both controller design and Kalman filter design. In Chapter 3 switching methods are introduced and tested using simulations. Possible problems that can occur during switching and the reasons they occur are analyzed. Two different methods are introduced to improve switching performance. A detailed switching method using Model Predictive Control (MPC) is developed in Chapter 4. First the application of MPC to tire force control is introduced. The advantages of using preview information about the switch in the MPC is shown. Different weightings of the MPC are investigated. Since the MPC requires information about all system states a Cubature Kalman filter is designed. Simulations are conducted for MPC switching using both the vehicle model developed in Chapter 2 and the detailed Volvo vehicle model (VTM). In Chapter 5 sigmoid functions are applied in switching from a Control Allocation (CA) controller to a rule-based controller. A CA failure scenario is investigated and various sigmoid function switching methods are analyzed. The conclusion of the thesis is in Chapter 6.

2

Vehicle Modeling

In this chapter, a longitudinal vehicle model is developed for use in the later chapters of the thesis.

2.1 Longitudinal Vehicle Model

The diagram of the model that is developed is shown in Figure 2.1. The velocity of the vehicle is v_{tr}. The vehicle consists of an electric drive front axle and an electric drive rear axle that can be controlled separately. The front electric motor has a constant rotational inertia, J_{m1}, and has an input τ_1 applied to it. The electric motor is assumed to be connected to a single front tire with a shaft of constant stiffness, c_{s1}, and constant damping, d_{s1}. The single front tire is assumed to represent both front tires. The front tire has a constant inertia of J_{t1} and the longitudinal force produced by the front tire is F_{t1}. The angular velocities of the front electric motor and the front tire are ω_{m1} and ω_{t1}, respectively. The rotational twist angle of the shaft that connects the front wheel to the front electric motor is θ_{s1}. The same parameters names and variable names are used for the rear axle with a subscript of "2". The front and rear tires have constant radius R. The vehicle has seven states that are shown in Equation 2.1.

$$x = \begin{bmatrix} v_{tr} \\ \omega_{m1} \\ \theta_{s1} \\ \omega_{t1} \\ \omega_{m2} \\ \theta_{s2} \\ \omega_{t2} \end{bmatrix} \tag{2.1}$$

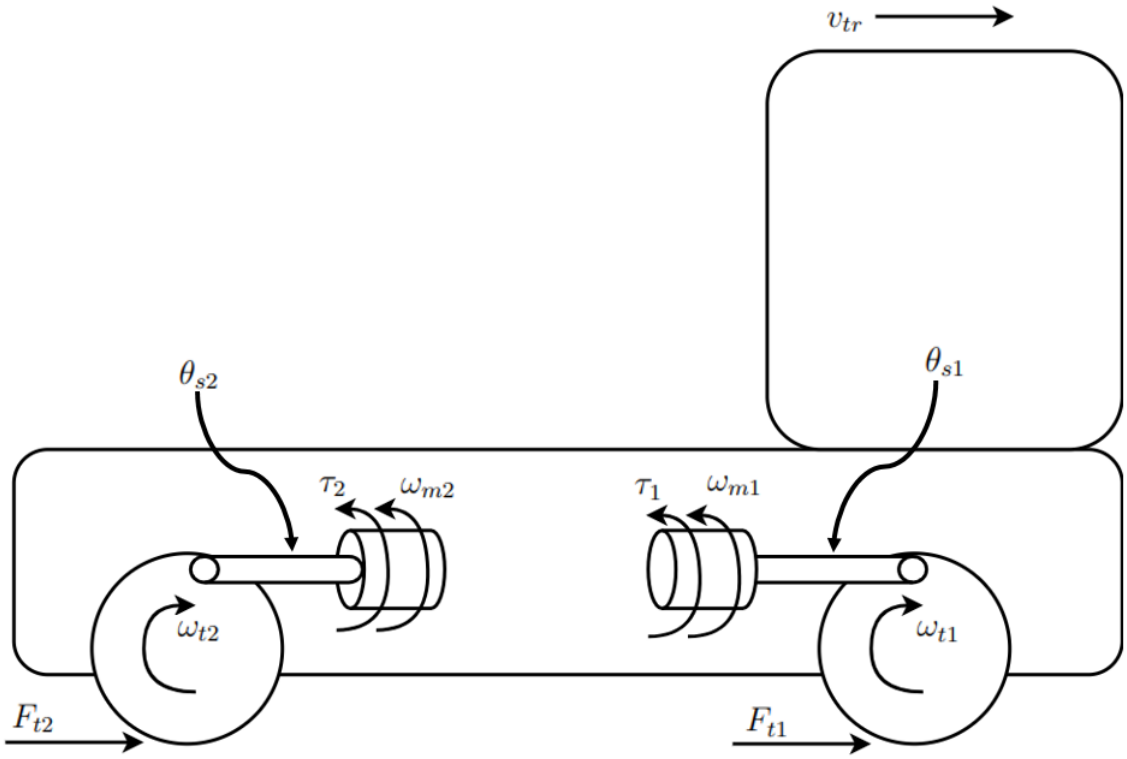

Figure 2.1: Longitudinal truck model diagram.

The longitudinal tire forces are calculated with the linear tire model shown in 2.2

$$F_{ti} = C_{xi} F_{zi} s_{xi} \tag{2.2}$$

where F_{ti} is the tire force, C_{xi} is the constant slip stiffness coefficient, F_{zi} is the constant normal tire force and s_{xi} is the tire slip. The subscript i is 1 for the front axle and 2 for the rear axle. The slip is calculated by using Equation 2.3.

$$s_{xi} = \frac{R \cdot \omega_{ti} - v_{tr}}{|v_{trss}|} \tag{2.3}$$

It should be noted that usually $R \cdot \omega_{ti}$ is used instead of v_{trss} in the denominator but since developing a linear time invariant system is the current goal, it is better to use v_{trss} since it changes slowly. Thus we assume v_{trss} is constant. The goal is to put the equations in the state space form shown in Equation 2.4.

$$\dot{x} = Ax + B_{full} u_{full} \tag{2.4}$$

It should be noted that matrices A and B_{full} are constant in Equation 2.4. Using Newton's laws the parts of Equation 2.4 can be calculated as the following:

$$\dot{x} = \begin{bmatrix} \dot{v}_{tr} \\ \dot{\omega}_{m1} \\ \dot{\theta}_{s1} \\ \dot{\omega}_{t1} \\ \dot{\omega}_{m2} \\ \dot{\theta}_{s2} \\ \dot{\omega}_{t2} \end{bmatrix} \tag{2.5}$$

$$A = \begin{bmatrix} \frac{-C_{x1}-C_{x2}}{m_{tr}v_{trss}} & 0 & 0 & \frac{C_{x1}R}{m_{tr}v_{trss}} & 0 & 0 & \frac{C_{x2}R}{m_{tr}v_{trss}} \\ 0 & \frac{-d_{s1}}{J_{m1}} & \frac{-c_{s1}}{J_{m1}} & \frac{d_{s1}}{J_{m1}} & 0 & 0 & 0 \\ 0 & 1 & 0 & -1 & 0 & 0 & 0 \\ \frac{C_{x1}R}{J_{t1}v_{trss}} & \frac{d_{s1}}{J_{t1}} & \frac{c_{s1}}{J_{t1}} & \frac{-d_{s1}v_{trss}-C_{x1}R^2}{J_{t1}v_{trss}} & 0 & 0 & 0 \\ 0 & 0 & 0 & 0 & \frac{-d_{s2}}{J_{m2}} & \frac{-c_{s2}}{J_{m2}} & \frac{d_{s2}}{J_{m2}} \\ 0 & 0 & 0 & 0 & 1 & 0 & -1 \\ \frac{C_{x2}R}{J_{t2}v_{trss}} & 0 & 0 & 0 & \frac{d_{s2}}{J_{t2}} & \frac{c_{s2}}{J_{t2}} & \frac{-d_{s2}v_{trss}-C_{x2}R^2}{J_{t2}v_{trss}} \end{bmatrix} \tag{2.6}$$

$$B_{full} = \begin{bmatrix} 0 & 0 & 1 \\ \frac{1}{J_{m1}} & 0 & 0 \\ 0 & 0 & 0 \\ 0 & 0 & 0 \\ 0 & \frac{1}{J_{m2}} & 0 \\ 0 & 0 & 0 \\ 0 & 0 & 0 \end{bmatrix} \tag{2.7}$$

$$u_{full} = \begin{bmatrix} \tau_1 \\ \tau_2 \\ -g \cdot sin(\theta) \end{bmatrix} \tag{2.8}$$

It should be noted that slip stiffness, C_i, has been used instead of slip stiffness coefficient, C_{xi} to make A easier to understand. The relationship is shown in Equation 2.9.

$$C_i = C_{xi}F_{zi} \tag{2.9}$$

Other than the two electric torque inputs to the system there is a gravity force input to the system depending on the slope of the road. The vehicle is assumed to be going uphill on a road with a slope of θ and g is the gravitational acceleration constant. It is possible to calculate tire forces using the standard state-space format shown in

$$y = Cx \tag{2.10}$$

where the tire forces are shown in Equation 2.11.

$$\begin{bmatrix} F_{t1} \\ F_{t2} \end{bmatrix} = \begin{bmatrix} \frac{-C_1}{v_{trss}} & 0 & 0 & \frac{C_1R}{v_{trss}} & 0 & 0 & 0 \\ \frac{-C_2}{v_{trss}} & 0 & 0 & 0 & 0 & 0 & \frac{C_2R}{v_{trss}} \end{bmatrix} \begin{bmatrix} v_{tr} \\ \omega_{m1} \\ \theta_{s1} \\ \omega_{t1} \\ \omega_{m2} \\ \theta_{s2} \\ \omega_{t2} \end{bmatrix} \tag{2.11}$$

3

Analysis of Controller Switching

In this chapter, the problems of switching controllers is analyzed from the perspective of control of heavy vehicles. Different methods of solving these problems are developed.

3.1 Switching Between Two PI Controllers

In this chapter the process of switching between two different controllers that have their own control loops in considered. Different switching cases are considered first and methods of improving the switching process in order of increasing complexity are shown afterwards. The switching process is shown with simulations using the VTM model which is a realistic simulation environment developed by Volvo AB that runs in Simulink. The goal is to show switching between systems where the controllers have their own dynamics. PI controllers are one of the simplest controllers that have dynamics because of the integral term. Therefore, the simulation is carried out for switching between two PI controllers. The goal of both PI controllers is to keep the vehicle traveling at constant velocity. However, the goal of Controller 1 is to use the front axle for 80% of the power and use the rear axle for 20% of the power. The goal of Controller 2 is to use the front axle for 40% of the power and use the rear axle for 60% of the power. The block diagram of the switching process is shown in Figure 3.1a. The online controller in the figure is Controller 1 and and the offline controller is Controller 2. The Vehicle is the VTM model and the estimator is simply the velocity measurement from the vehicle. The reference is a velocity reference of 40km/h. The vehicle is traveling up a hill with a 5 degree slope. The actuator torques for an instant switch are shown in Figure 3.1b. In the figure, Stage 1 is shown as the steady state motion of the vehicle before the switch and Stage 2 is the motion of the vehicle after the switch. The figure shows that when the switch to Controller 2 occurs, the actuator torques become zero and then start increasing. This happens because the controller has zero initial conditions and the integrator takes some time to reach steady state. Ultimately, the actuator torques reach the correct steady state values.

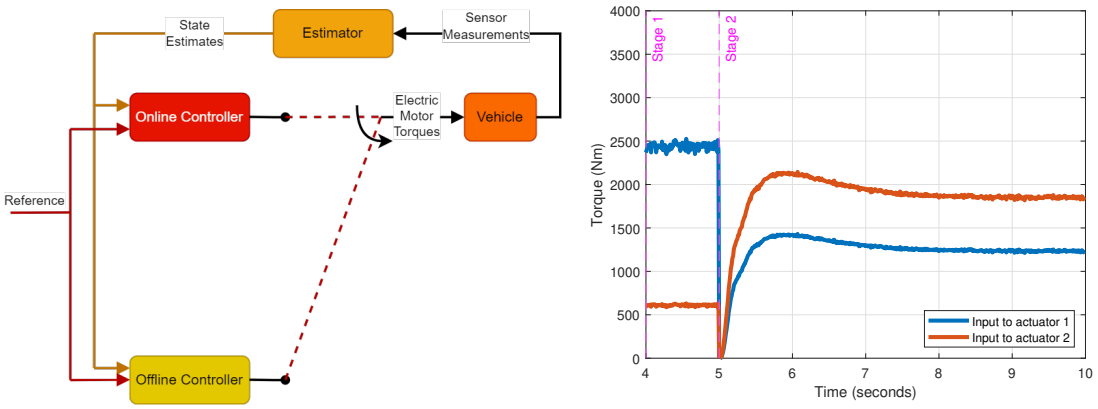

(a) Block diagram. **(b)** Actuator torques.

Figure 3.1: Switching between Controller 1 and Controller 2 process.

The results of this type of switching for tire forces are shown in Figure 3.2a and the velocity is shown in Figure 3.2b. Figure 3.2a shows that the tire forces become close to zero for a short while before they reach the correct values. The decrease in the tire forces results in a decrease in the velocity before it goes back to the original value as shown in Figure 3.2b.

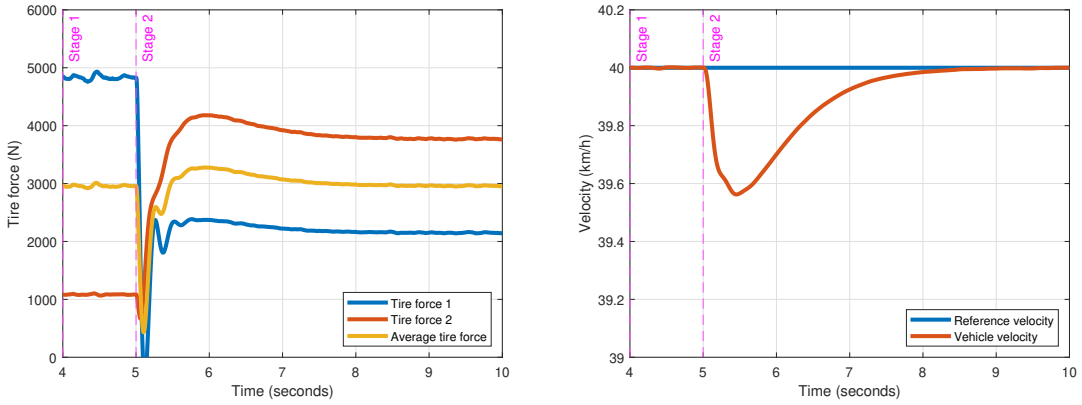

(a) Tire forces. **(b)** Velocity.

Figure 3.2: Switching between Controller 1 and Controller 2 results.

When sending requests to actuators it is possible for the actuators to take time to respond. In previous simulations we assumed electric motors were used as actuators. The response time of electric motors is relatively quick when compared with the response time of the rest of the system and can be neglected. However, when for example the switch it done to the brake system of the vehicle there is a delay that should be taken into account. In the next simulations it is assumed that the actuators that Controller 2 controls have a 0.2 second dead time. Repeating the same switching simulations as before but with a 0.2 second delay in the actuator torque, the results in Figure 3.3 are obtained. There is a 0.2 second period where

no torque is produced by the actuators. Afterwards, actuator torques are produced but they are quite oscillatory.

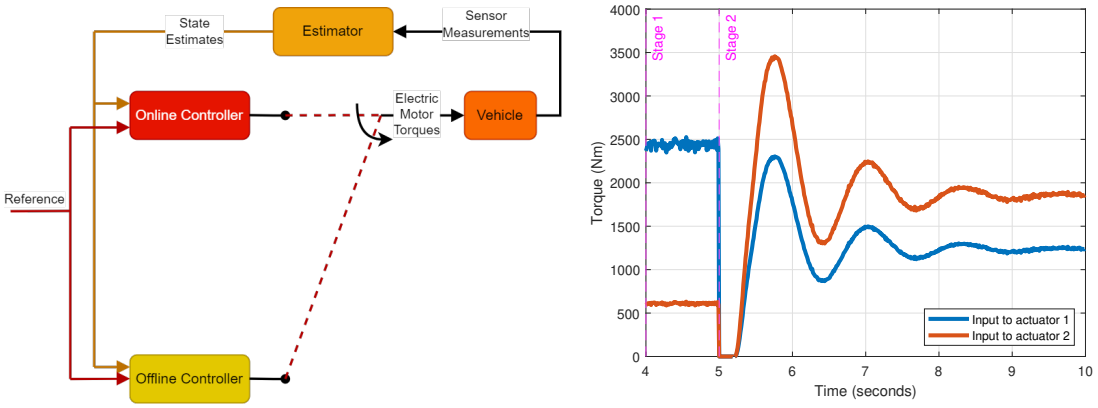

(a) Block diagram. **(b)** Actuator torques.

Figure 3.3: Switching between Controller 1 and Controller 2 process with 0.2 second actuator delay.

The tire force and velocity results for the actuators with 0.2 second delay are shown in Figure 3.4a and 3.4b, respectively. The tire forces reach very low levels and take more time to reach the steady state values than in the previous simulation. Because of the larger and longer decrease in the tire forces, the velocity decreases to lower levels than before resulting in poorer performance. It should be noted that for these simulations the torques are positive and when no torque is produced the vehicle slows because of the delay. If the goal was to test switching to a braking system, the simulation would have to be slightly different and the velocity would increase during the break in the tire torque. For example, if the vehicle was traveling downhill and Controller 1 was keeping the vehicle velocity constant using negative motor torques and one was to switch to a mechanical braking system which lead to a stop in the negative torque for a short while this would have resulted in an increase of the speed of the vehicle.

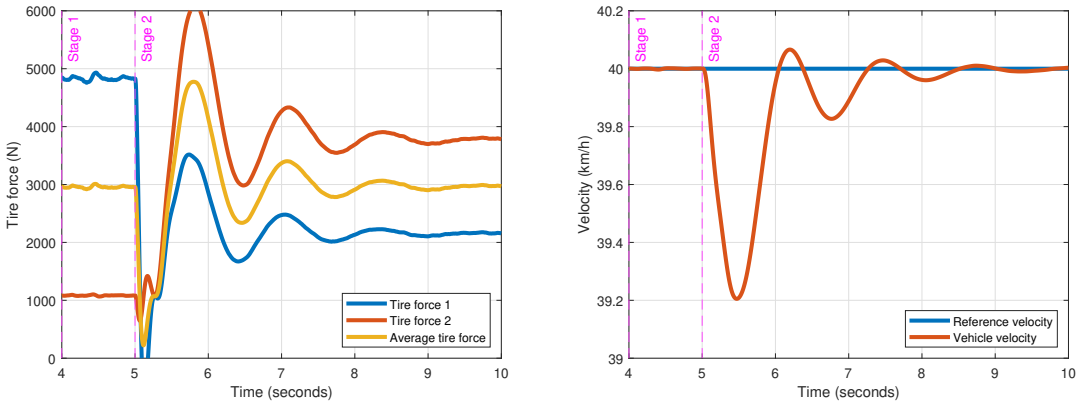

(a) Tire forces. **(b)** Velocity.

Figure 3.4: Switching between Controller 1 and Controller 2 results with 0.2 second actuator delay.

3.2 Switching Between Two PI Controllers by Flip-Flopping

In the previous section, switching from one PI controller to another PI controller was introduced. It is possible that switching back to the original controller is necessary. Some unexpected behaviour may occur if switching back occurs quickly. Furthermore, switching back and forth quickly, or flip-flopping can also result in problems. This possibility is investigated for different switching intervals in this section. The same controllers as in the previous section with no actuator delay are used in the simulations. Actuator torque requests for flip-flop switching with a 1 second interval is shown in Figure 3.5a. The corresponding tire forces are shown in Figure 3.5b. The figures show that the system approximately reaches steady state after 1 second. There is overshoot and some oscillations after each switch but the system remains stable.

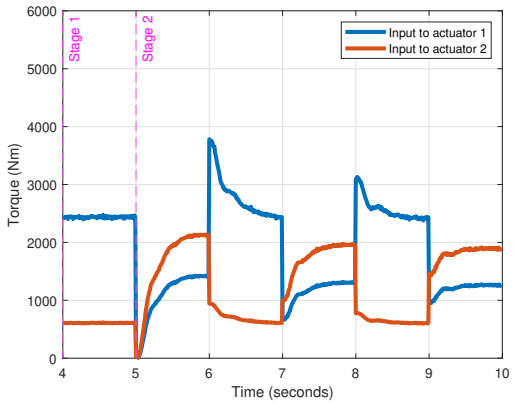

(a) Actuator Torques.

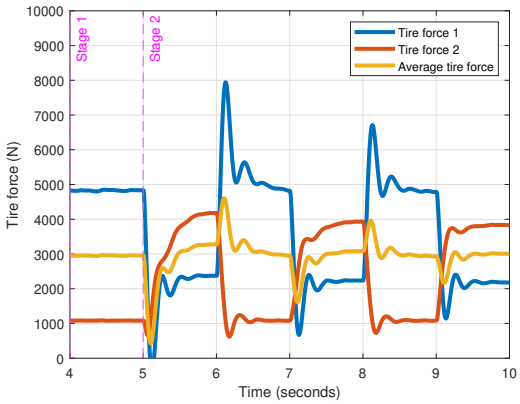

(b) Tire forces.

Figure 3.5: Switching between Controller 1 and Controller 2 with 1 second intervals.

The actuator torque requests for switching with 0.5 second intervals is shown in Figure 3.6a whereas the corresponding tire forces are shown in Figure 3.6b. It is observed that the switches occur before the system reaches steady state. Furthermore, larger overshoots occur after each switch for both the actuator torque requests and tire forces. However, the switching system is stable according to the simulations.

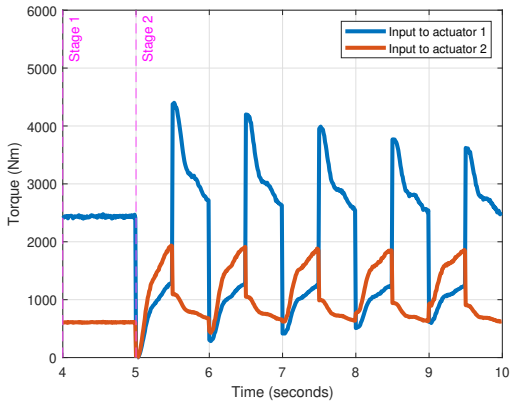

(a) Actuator Torques.

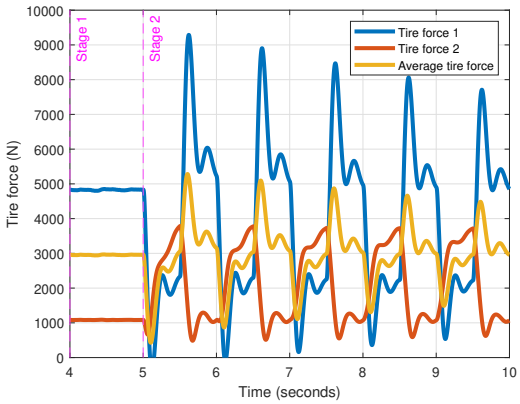

(b) Tire forces.

Figure 3.6: Switching between Controller 1 and Controller 2 with 0.5 second intervals.

The actuator torque requests for switching with 0.05 second intervals is shown in Figure 3.7a whereas the corresponding tire forces are shown in Figure 3.7b. The actuator torque requests occur as oscillations at the frequency of switching. The amplitudes of the oscillations are relatively large. The tire forces also have oscillations at this frequency. However, the amplitudes of the oscillations are relatively small when compared with the actuator torque requests. It is suspected that the

oscillations are damped as the actuator torques move through the drivetrain and reach the tires.

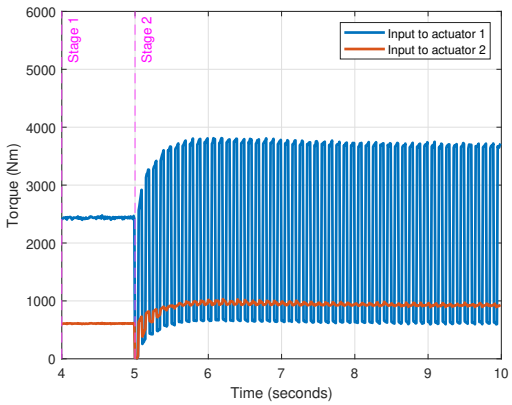

(a) Actuator Torques.

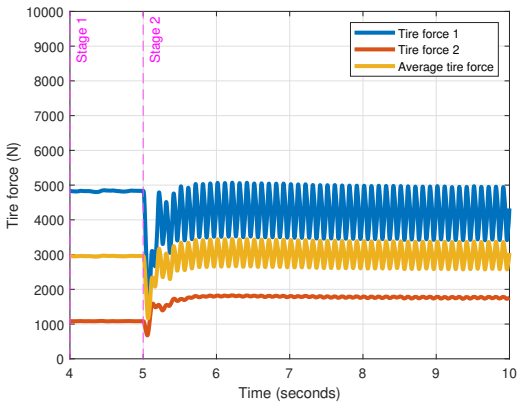

(b) Tire forces.

Figure 3.7: Switching between Controller 1 and Controller 2 with 0.05 second intervals.

The velocity of the vehicle for 1, 0.5 and 0.05 second switching intervals are shown in Figure 3.8a, Figure 3.8b and Figure 3.9, respectively. There are oscillations in the velocities corresponding to the frequency of each switching interval. The amplitudes of the oscillations are similar in size for the 1 and 0.5 second switching intervals whereas they are relatively small for the 0.05 second switching interval.

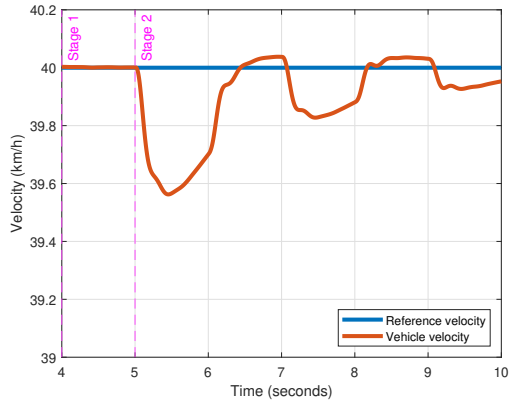

(a) 1 second interval.

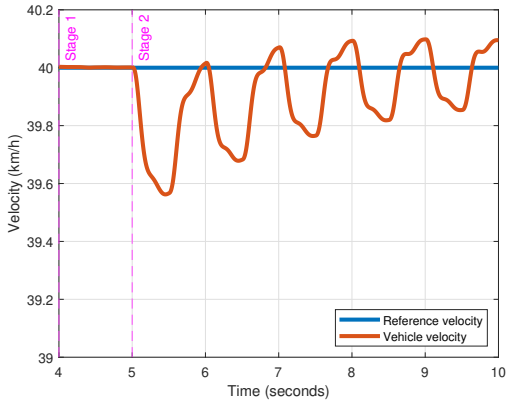

(b) 0.5 second interval.

Figure 3.8: Vehicle velocity for different switching intervals.

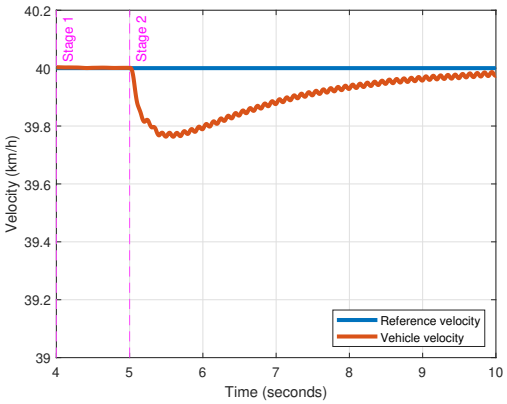

Figure 3.9: Vehicle velocity for 0.05 second switching interval.

3.3 Model-Based Warm Start Switching

It was seen in the previous section that the starting the offline controller with zero initial conditions results in a deterioration of the performance. It is possible to have the offline controller connected to a model of the real system so that it is prepared to be connected to the real system. This methodology is shown in Figure 3.10a. Warm start switching is the name given to this method here. In this way the initial conditions of the controller are prepared to control the vehicle model just like it is controlling the real system. It is expected that the performance quality will depend on how well the model matches the real system. To alleviate this problem, the real system parameters can be estimated and updated for the model. In the example here, the tire stiffnesses are estimated by a Cubature Kalman filter. The Cubature Kalman filter is introduced in Chapter 4. The reason for the choice of tire parameters as the estimation parameter is that tire parameters are the most difficult to know whereas other parameters are generally fixed or can be measured. The details of the estimation are explained in the section about state and parameter estimation in Chapter 4. Figure 3.10b shows the results of the simulation for the actuator torques. In Stage 1, there are two control loops where each controller is controlling its own model. In Stage 2 Controller 1 is disconnect from the real system. Furthermore, Controller 2 is connected to the real system and also starts using the feedback information from the real system at the same time. The results are quite good since the oscillations after the switch are very small and steady is reached at about 0.3 seconds after the switch. This means that the model matches the real vehicle quite well. It should be noted that the real vehicle is the VTM model and the model is the 7 state model previously developed in Chapter 2.

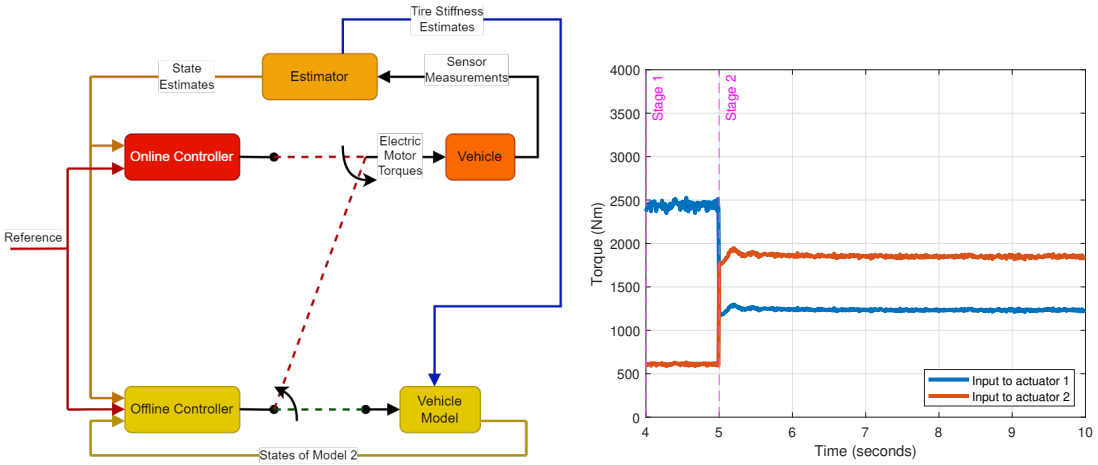

(a) Block diagram. **(b)** Actuator torques.

Figure 3.10: Simple switching between Controller 1 and Controller 2 process with 0.2 second actuator delay.

The tire forces and the velocity of the vehicle for the switch where the offline controller is initially connected to a model is shown in Figure 3.11a and 3.11b. The tire forces have small oscillations about the steady state values they should reach. Figure 3.11a shows the average tire forces as well which change very little from its value previous to the switch. This is quite good and the result can be seen in 3.11b where the velocity of the vehicle changes very little during the switching process.

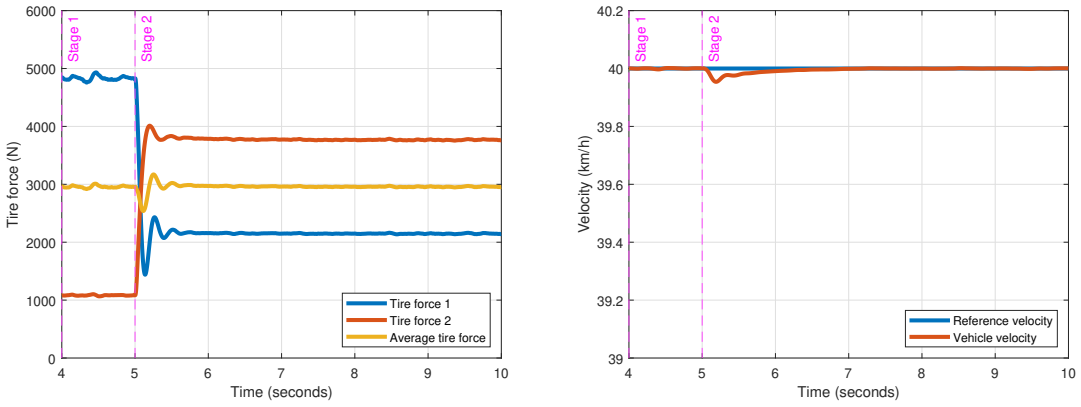

(a) Tire forces. **(b)** Velocity.

Figure 3.11: Simple switching between Controller 1 and Controller 2 with model results.

As in the Section 3.1, the effect of having 0.2 second delay in the actuator is simulated and shown in Figure 3.12. There is some deterioration in the performance. It can be seen that the control input to the actuator does not change for 0.2 seconds even though the switch has occurred.

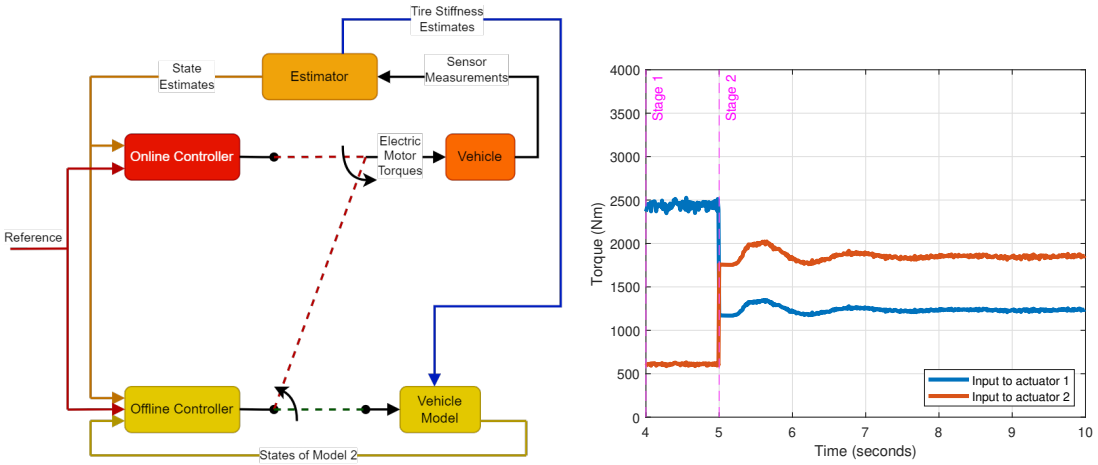

(a) Block diagram. **(b)** Actuator torques.

Figure 3.12: Simple switching between Controller 1 and Controller 2 process with 0.2 second actuator delay.

The effect of the actuator delay can be seen in the tire forces shown in Figure 3.13a where the tire forces decrease during the time where slightly inaccurate actuator torques are produced because of the delay in actuator torque production. This results in deterioration of velocity tracking performance as seen in Figure 3.13b compared to when there was no actuator delay.

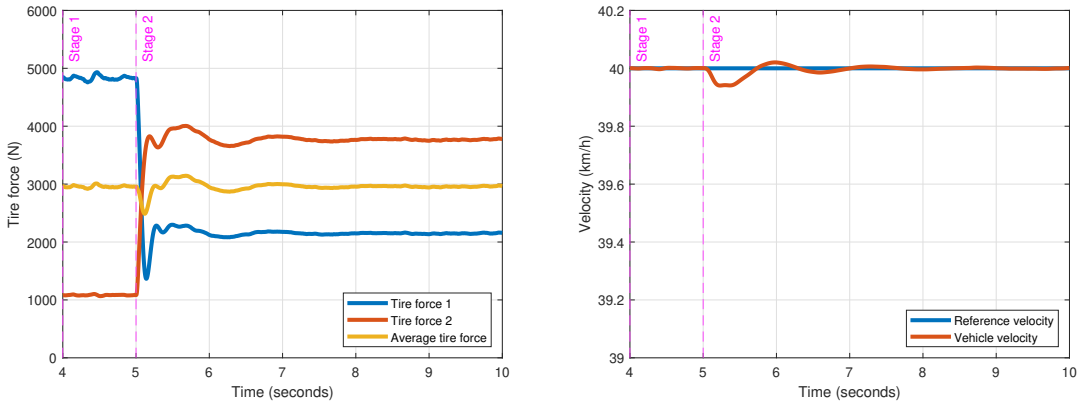

(a) Tire forces. **(b)** Velocity.

Figure 3.13: Simple switching between Controller 1 and Controller 2 with 0.2 second actuator delay and with model results.

3.4 Model-Based Warm Start Switching With Interpolation

Sudden switching can result in rapid changes in requests and actuator torques. It is possible to slow this process using different methods. The method used in this

section is linear interpolation between the outputs of the online controller to the outputs of the offline controller. The switching occurs in 3 stages. In Stage 1 both controllers are working in their own loops to control the real vehicle and the vehicle model separately. This stage is the same as Stage 1 in simple switching and is shown in Figure 3.14a. Stage 3 is the final stage after the linear interpolation has occurred and Controller 2 is fully connected to the real system. The block diagram of Stage 3 is shown in 3.14b.

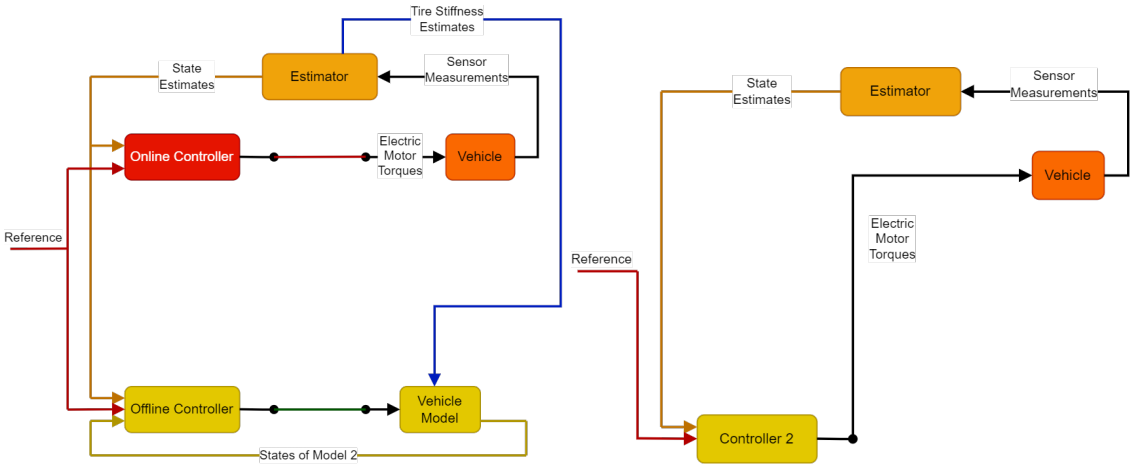

(a) Stage 1. **(b)** Stage 3.

Figure 3.14: Linear interpolation switching between Controller 1 and Controller 2 Stage 1 and Stage 3.

The block diagram of the interpolation switching process is shown in Figure 3.15a. The output of Controller 1 is multiplied by gain G1 and added to the output of the Controller 2 which is multiplied by gain G2. The variation of the G1 and G2 are shown in Figure 3.15b. Gain G1 decreases from 1 to 0 linearly simultaneously as gain G2 increases from 0 to 1.

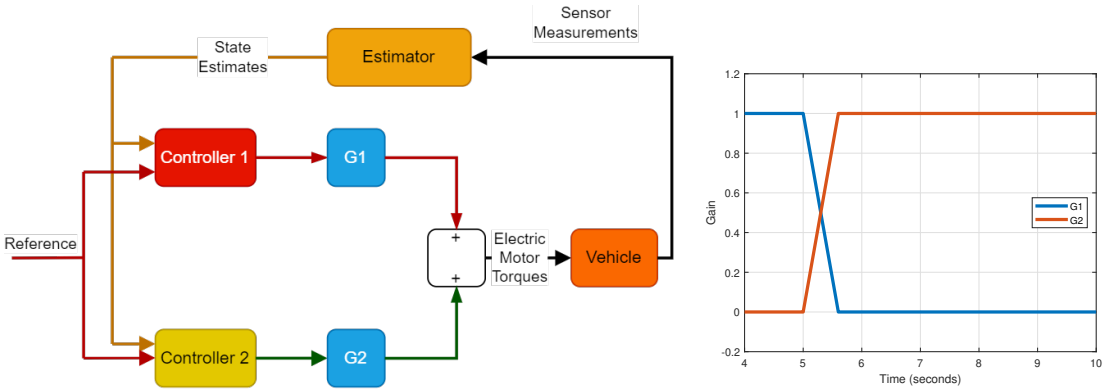

(a) Stage 2. **(b)** Interpolation gain variation.

Figure 3.15: Linear interpolation switching between Controller 1 and Controller 2.

The actuator torque during Stage 1, 2 and 3 are shown in Figure 3.16a. It is observed

that the torque switch in the actuators occurs without oscillations. It should be noted that during the linear interpolation switching both controllers continue to be connected to the real vehicle and continue to change their respective outputs. The change the outputs of Controller 1 and Controller 2 during the switch can be seen in Figure 3.16b and Figure 3.16c, respectively.

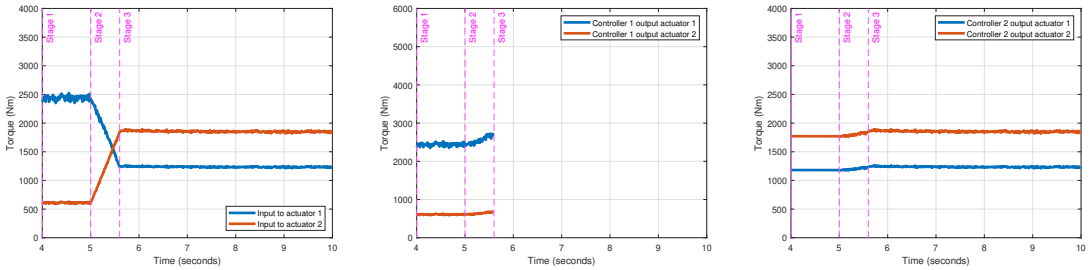

(a) Actuator torque. **(b)** Controller 1 output. **(c)** Controller 2 output.

Figure 3.16: Actuator torques during linear interpolation switching between Controller 1 and Controller 2 Stage 2.

The tire forces for linear interpolation switching are shown in Figure 3.17a. The figure shows that the switching is smooth with very little oscillations. The velocity during the linear interpolation switching shown in Figure 3.17b are also very good because there is very little change in the vehicle velocity during the switching process.

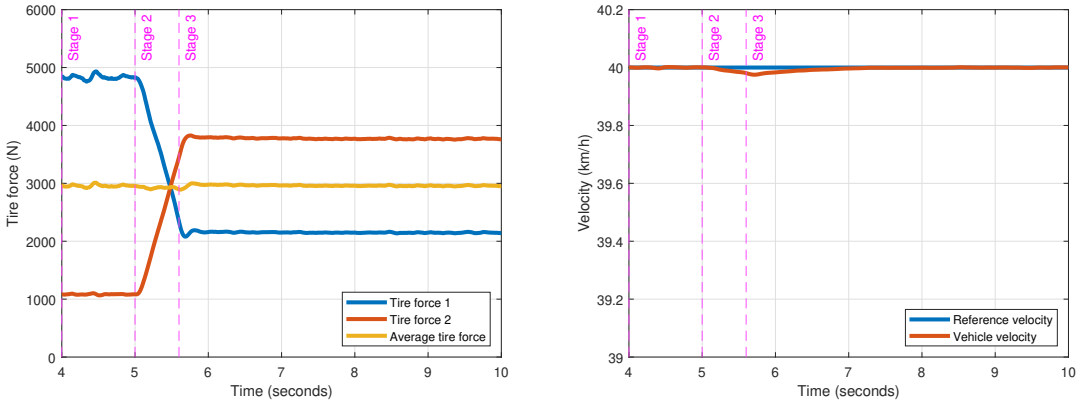

(a) Tire forces. **(b)** Velocity.

Figure 3.17: Linear interpolation switching between Controller 1 and Controller 2 with model results.

The actuator torques when there is delay in the actuators that Controller 2 is connected to are shown in Figure 3.18a. Some oscillations are observed after the switch which means that actuator delay causes deterioration of the performance of linear interpolation switching as well. Figure 3.18b and 3.18c show the controller outputs of the Controller 1 and Controller 2 respectively for this simulation. Oscillations are

observed in the output of Controller 2 because of the delay in the actuators that it is connected to.

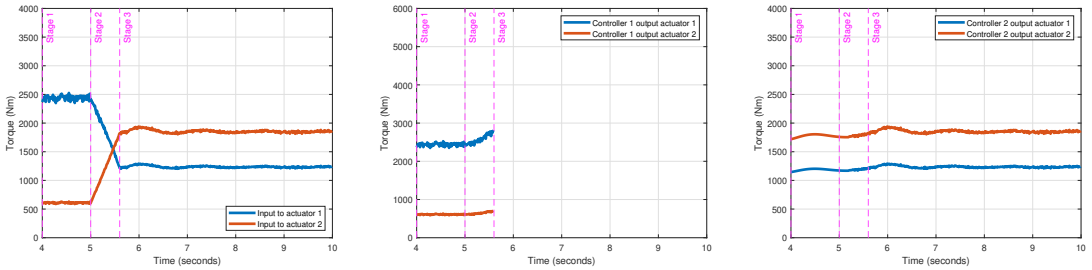

(a) Actuator torque. **(b)** Controller 1 output. **(c)** Controller 2 output.

Figure 3.18: Actuator torques during linear interpolation switching between Controller 1 and Controller 2 with actuator delay.

The effect of actuator delay on tire forces during linear interpolation switching can be seen in Figure 3.19a. Although the switching process is smooth some small oscillations occur after the switching process is over. The switching velocity performance also deteriorates slightly because of the actuator delay but can be considered to be quite good.

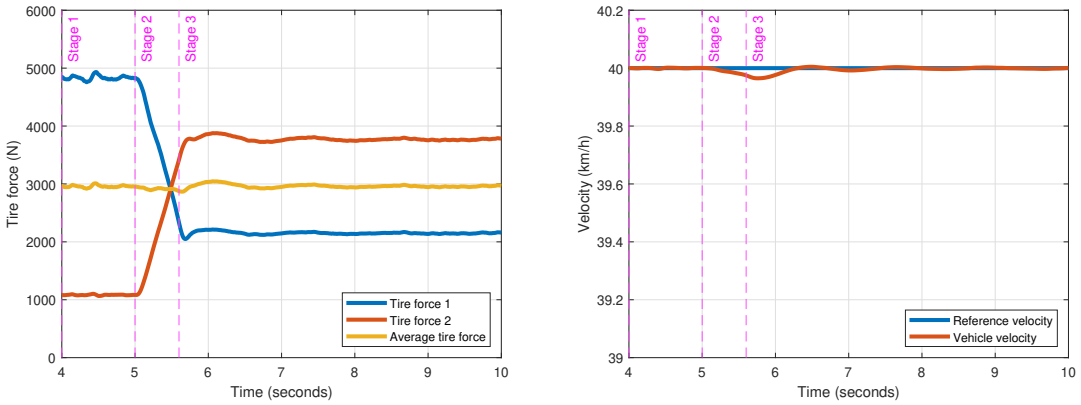

(a) Tire forces. **(b)** Velocity.

Figure 3.19: Linear interpolation switching between Controller 1 and Controller 2 with actuator delay.

4

Controller Switching Using Model Predictive Control

In this chapter, the application of model predictive control to the controller switching problem is analyzed.

4.1 Tire Force Tracking Using Model Predictive Control

4.1.1 Longitudinal Vehicle Control Using Tire Force Tracking

In this section the vehicle model equations are put into a form for controlling the tire forces of the longitudinal model developed in Chapter 2. A common method of for tracking references using state-space methods is to add integrator states. The addition of integrator states in discrete time is shown in Equations 4.1.

$$\begin{bmatrix} x(k+1) \\ x_{int}(k+1) \end{bmatrix} = \begin{bmatrix} A_d & 0 \\ -C \cdot T & I \end{bmatrix} \begin{bmatrix} x(k) \\ x_{int}(k) \end{bmatrix} + \begin{bmatrix} B_d \\ 0 \end{bmatrix} \begin{bmatrix} \tau_1(k) \\ \tau_2(k) \\ -g \cdot sin(\theta(k)) \end{bmatrix} + \begin{bmatrix} 0 \\ I \cdot T \end{bmatrix} \begin{bmatrix} F_{t1ref}(k) \\ F_{t2ref}(k) \end{bmatrix} \quad (4.1)$$

where A_d and B_d are discretized versions of A and B_{full}. A and B_{full} are the continuous time model matrices derived in Chapter 2. Going from continuous time to discrete time can be achieved exactly by assuming that the inputs are constant within sampling time T [20]. The specific sample is denoted with k. The front and rear reference tire forces are $F_{t1ref}(k)$ and $F_{t2ref}(k)$, respectively. The extended state vector is shown in Equations 4.2 where the integrals of the tire force errors F_{t1int} and F_{t2int} are added as extra states.

$$x(k) = \begin{bmatrix} v_{tr}(k) \\ \omega_{m1}(k) \\ \theta_{s1}(k) \\ \omega_{t1}(k) \\ \omega_{m2}(k) \\ \theta_{s2}(k) \\ \omega_{t2}(k) \\ F_{t1int}(k) \\ F_{t2int}(k) \end{bmatrix} \tag{4.2}$$

The integration can be calculated in discrete time as in Equations 4.3 and 4.4.

$$F_{t1int}(k+1) = (F_{t1ref}(k) - F_{t1}(k)) \cdot T + F_{t1int}(k) \tag{4.3}$$

$$F_{t2int}(k+1) = (F_{t2ref}(k) - F_{t2}(k)) \cdot T + F_{t2int}(k) \tag{4.4}$$

$F_{t1}(k)$ and $F_{t2}(k)$ are calculated in Equation 4.5.

$$\begin{bmatrix} F_{t1}(k) \\ F_{t2}(k) \end{bmatrix} = \begin{bmatrix} \frac{-C_1}{v_{trss}} & 0 & 0 & \frac{C_1 R}{v_{trss}} & 0 & 0 & 0 \\ \frac{-C_2}{v_{trss}} & 0 & 0 & 0 & 0 & 0 & \frac{C_2 R}{v_{trss}} \end{bmatrix} \begin{bmatrix} v_{tr}(k) \\ \omega_{m1}(k) \\ \theta_{s1}(k) \\ \omega_{t1}(k) \\ \omega_{m2}(k) \\ \theta_{s2}(k) \\ \omega_{t2}(k) \end{bmatrix} \tag{4.5}$$

In this form the system can be controlled using Linear Quadratic Regulator Control (LQR). However, MPC is used here because it has some advantages over the LQR.

4.1.2 Longitudinal Vehicle Control Using Model Predictive Control

In this section a Model Predictive Controller (MPC) is developed for controlling the tire forces. Some of the commonly used advantages MPCs are being able to place constraints on the system inputs and states. Here, the advantage of taking into account future disturbances (reference inputs) will be used.

MPC is a control method based on optimization. The goal is to minimize the cost function over a prediction horizon N. The cost function is

$$V_N(x(0), u(0:N-1)) = x^T(N) P_f x(N) + \sum_{i=0}^{N-1} (x^T(i) Q x(i) + u^T(i) R u(i) \tag{4.6}$$

where $x(k)$ is as shown in Equation 4.2 for this example and $u(k)$ is as shown in Equation 4.7 for this example.

$$u(k) = \begin{bmatrix} \tau_1(k) \\ \tau_2(k) \end{bmatrix} \tag{4.7}$$

The R matrix is used to weight the actuator torques. When the values of R are increased, the cost of the actuator inputs increases. This results in a decrease in the amount of control input to the system to minimize the cost function. The Q matrix is used to weight individual states and P_f is used to weight the individual states in the final step of the optimization horizon. The cost function is subject to inequality constraints $H \leq f$ and equality constraints $H_{eq}x = f_{eq}$. The equality constraints are used to make sure Equation 4.1 holds for the optimization because $x(k+1) = Ax(k) + Bu(k)$ must hold for the whole optimization horizon. The inequality constraints can be used to put constraints on the actuator outputs and on the states.

For the vehicle tire force control example considered in this section, the goal is to minimize the error in the integral of the tire forces. To achieve this goal the cost matrix is weighted to minimize these tracking error integrals using

$$Q_1 = \begin{bmatrix} 0 & 0 & 0 & 0 & 0 & 0 & 0 & 0 & 0 \\ 0 & 0 & 0 & 0 & 0 & 0 & 0 & 0 & 0 \\ 0 & 0 & 0 & 0 & 0 & 0 & 0 & 0 & 0 \\ 0 & 0 & 0 & 0 & 0 & 0 & 0 & 0 & 0 \\ 0 & 0 & 0 & 0 & 0 & 0 & 0 & 0 & 0 \\ 0 & 0 & 0 & 0 & 0 & 0 & 0 & 0 & 0 \\ 0 & 0 & 0 & 0 & 0 & 0 & 0 & 0 & 0 \\ 0 & 0 & 0 & 0 & 0 & 0 & 0 & W_8 & 0 \\ 0 & 0 & 0 & 0 & 0 & 0 & 0 & 0 & W_9 \end{bmatrix} \tag{4.8}$$

The cost matrix for the inputs is designated as

$$R_1 = \begin{bmatrix} W_{R1} & 0 \\ 0 & W_{R2} \end{bmatrix} \tag{4.9}$$

The effects of different weighting choices are shown in Section 4.1.4.

4.1.3 The Advantages of Preview Information

In this section, switching between two different tire force references is focused on. There are two possible variations for this switch to occur. It is possible that the time that the switch will occur is known before the switch happens. It is also possible that there is no knowledge beforehand and the tire force references suddenly change. The time history of the tire force reference is shown in Figure 4.1. Now consider that the current time is 1.6 seconds and the MPC has a prediction horizon of N=30 or 0.3 seconds. If the controller does not have information about the coming switch the prediction is calculated according to a constant reference as shown in in Figure 4.2a. However, if the controller does have information that a switch is coming as shown in Figure 4.2b, then the switch in the reference is used in the calculation of the controller throughout the horizon.

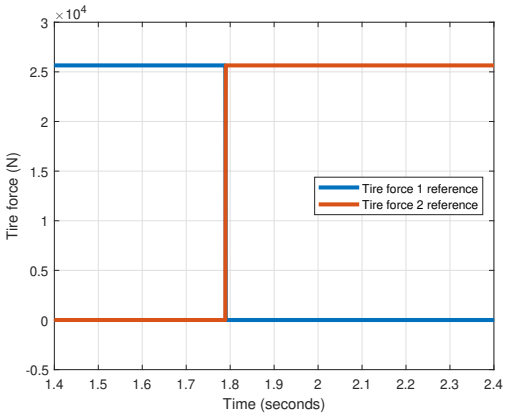

Figure 4.1: Reference tire force for whole simulation.

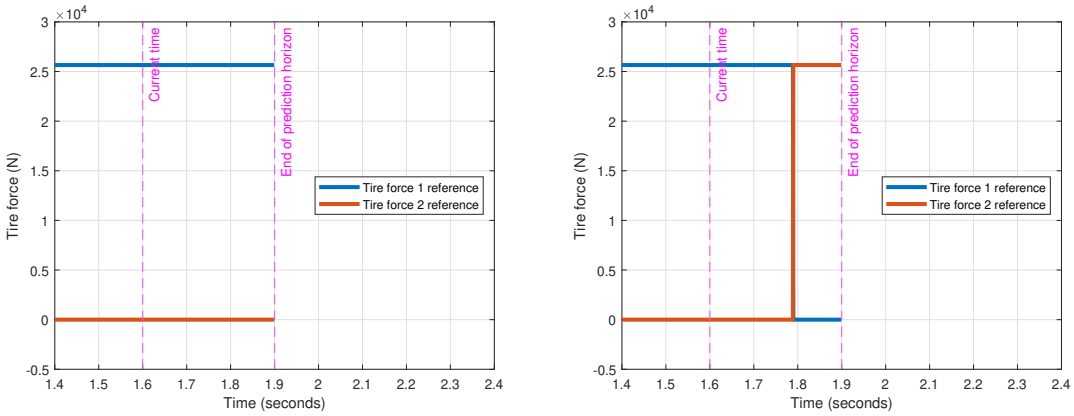

(a) With preview. **(b)** Without preview.

Figure 4.2: Reference tire force for current time = 1.6 seconds.

To compare the different responses for the MPC with and without preview, the controller outputs, tire forces and vehicle acceleration are plotted. The controller outputs which are assumed to also be the actuator torques are shown in Figure 4.3. The simulation shows that when the controller has preview information, the actuator slowly starts producing torque when it receives information that a switch is coming. However, the controller that does not have preview information suddenly produces large torques when the reference tire force changes. The tire forces that result from these actuator torques are shown in Figure 4.4*a*. The figure shows that the preview controller is much more capable at following the reference tire forces. On the other hand, the controller without preview information has large oscillations and overshoot during switching. The difference in the acceleration performance of both controllers are shown in Figure 4.4*b*. During switching from one axle to the other oscillations occur because the tire parameters of the two axles are different. The oscillation magnitudes are larger without preview when compared to the oscillation magnitudes with preview. As expected, small oscillations starts before switching time for the controller with preview but large oscillation start right at switching time for the controller without preview.

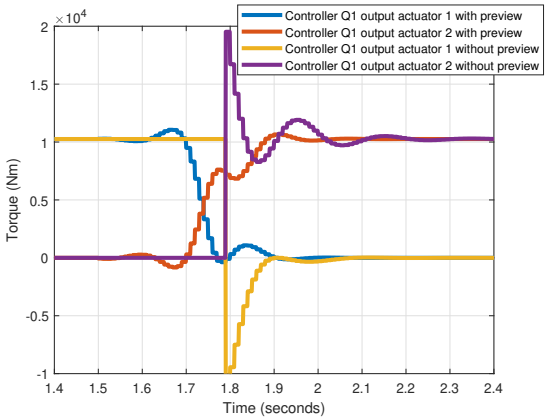

Figure 4.3: Actuator torque with and without preview.

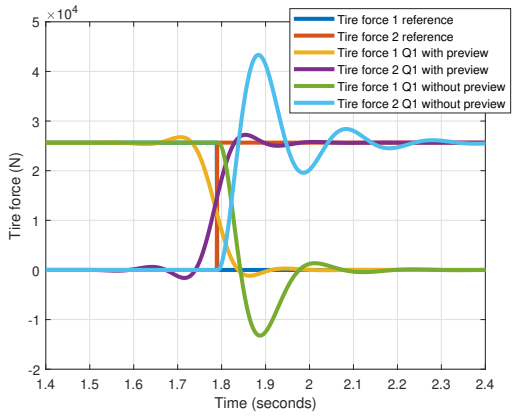

(a) Tire forces.

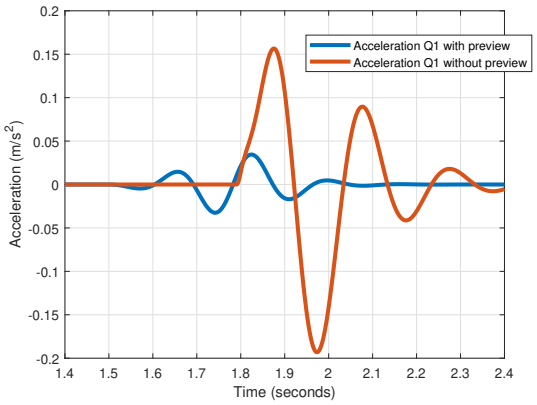

(b) Acceleration.

Figure 4.4: Simulation with and without preview.

4.1.4 Effects of Different Controller Weightings

Using an MPC provides flexibility in controller design and it is possible to focus on different metrics to achieve different goals. To focus on different metrics it is possible to use different Q matrices to weight states differently depending on the preferences of the control designer. It is also possible to add more metrics as states and put costs on those states depending on how much the control designer wants to focus on those metrics. This is why several different MPC controllers are developed in this chapter to compare the performance of different MPC weightings. The controller designed using the Q_1 weighting in Equation 4.8 is named Controller Q1. Since the advantage of preview information was observed in the previous section all of the controllers used in the following comparison use preview information. In the design of Controller Q2, 2 more states that are the error between the reference tire force

and the real tire force are added as

$$x(k) = \begin{bmatrix} v_{tr}(k) \\ \omega_{m1}(k) \\ \theta_{s1}(k) \\ \omega_{t1}(k) \\ \omega_{m2}(k) \\ \theta_{s2}(k) \\ \omega_{t2}(k) \\ F_{t1int}(k) \\ F_{t2int}(k) \\ F_{t1p}(k) \\ F_{t2p}(k) \end{bmatrix} \quad (4.10)$$

where F_{t1p} and F_{t2p} are the tracking errors of the the tire forces calculated in Equations 4.11 and 4.12.

$$F_{t1p}(k) = F_{t1ref}(k) - F_{t1}(k) \quad (4.11)$$

$$F_{t2p}(k) = F_{t2ref}(k) - F_{t2}(k) \quad (4.12)$$

The cost matrix is weighted to minimize these tracking errors and their integrals as shown in Equation 4.13.

$$Q_2 = \begin{bmatrix} 0&0&0&0&0&0&0&0&0&0&0 \\ 0&0&0&0&0&0&0&0&0&0&0 \\ 0&0&0&0&0&0&0&0&0&0&0 \\ 0&0&0&0&0&0&0&0&0&0&0 \\ 0&0&0&0&0&0&0&0&0&0&0 \\ 0&0&0&0&0&0&0&0&0&0&0 \\ 0&0&0&0&0&0&0&0&0&0&0 \\ 0&0&0&0&0&0&0&W_8&0&0&0 \\ 0&0&0&0&0&0&0&0&W_9&0&0 \\ 0&0&0&0&0&0&0&0&0&W_{10}&0 \\ 0&0&0&0&0&0&0&0&0&0&W_{11} \end{bmatrix} \quad (4.13)$$

Controller Q1 can be thought of as similar to an integral controller whereas Controller Q2 can be thought of as similar to a proportional integral (PI) controller. Figure 4.5 and Figure 4.6 show the simulations that compare Controller Q1 and Controller Q2. According to Figure 4.5 Controller Q2 produces faster actuator responses compared to Controller Q1. Figure 4.6 shows that the tire force response is slightly faster with less percent overshoot. Furthermore, the acceleration is slightly less for Controller Q2 when compare with Controller Q1, which is an advantage.

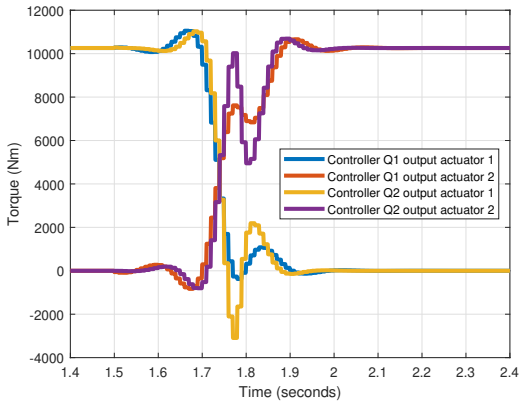

Figure 4.5: Actuator torques for Controller Q1 and Controller Q2.

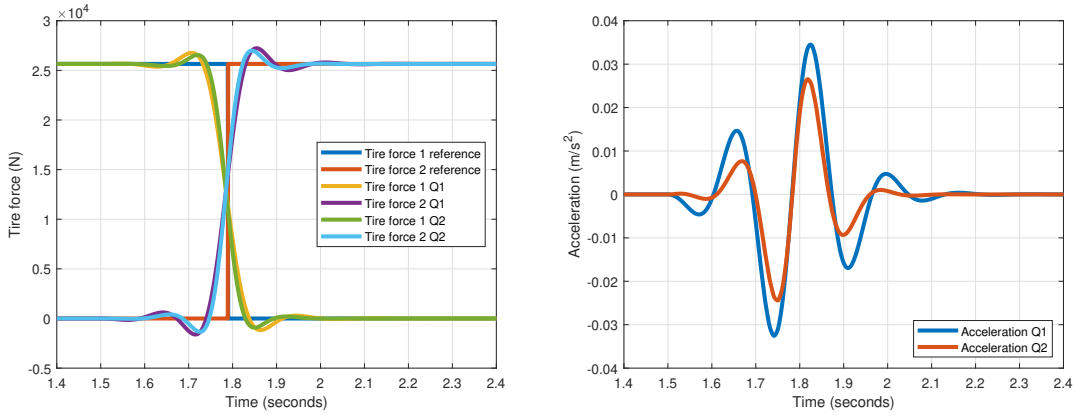

(a) Tire forces. **(b)** Acceleration.

Figure 4.6: Simulation for Controller Q1 and Controller Q2.

In the design of Controller Q3, the acceleration state, $a_{tr}(k)$ is added, which is a derivative of the longitudinal velocity as shown in Equation 4.14.

$$x(k) = \begin{bmatrix} v_{tr}(k) \\ \omega_{m1}(k) \\ \theta_{s1}(k) \\ \omega_{t1}(k) \\ \omega_{m2}(k) \\ \theta_{s2}(k) \\ \omega_{t2}(k) \\ F_{t1i}(k) \\ F_{t2i}(k) \\ F_{t1p}(k) \\ F_{t2p}(k) \\ a_{tr}(k) \end{bmatrix} \tag{4.14}$$

The cost matrix is weighted to minimize the tracking errors, their integrals and the acceleration as shown in Equation 4.15.

$$Q_3 = \begin{bmatrix} 0 & 0 & 0 & 0 & 0 & 0 & 0 & 0 & 0 & 0 & 0 & 0 \\ 0 & 0 & 0 & 0 & 0 & 0 & 0 & 0 & 0 & 0 & 0 & 0 \\ 0 & 0 & 0 & 0 & 0 & 0 & 0 & 0 & 0 & 0 & 0 & 0 \\ 0 & 0 & 0 & 0 & 0 & 0 & 0 & 0 & 0 & 0 & 0 & 0 \\ 0 & 0 & 0 & 0 & 0 & 0 & 0 & 0 & 0 & 0 & 0 & 0 \\ 0 & 0 & 0 & 0 & 0 & 0 & 0 & 0 & 0 & 0 & 0 & 0 \\ 0 & 0 & 0 & 0 & 0 & 0 & 0 & 0 & 0 & 0 & 0 & 0 \\ 0 & 0 & 0 & 0 & 0 & 0 & 0 & W_8 & 0 & 0 & 0 & 0 \\ 0 & 0 & 0 & 0 & 0 & 0 & 0 & 0 & W_9 & 0 & 0 & 0 \\ 0 & 0 & 0 & 0 & 0 & 0 & 0 & 0 & 0 & W_{10} & 0 & 0 \\ 0 & 0 & 0 & 0 & 0 & 0 & 0 & 0 & 0 & 0 & W_{11} & 0 \\ 0 & 0 & 0 & 0 & 0 & 0 & 0 & 0 & 0 & 0 & 0 & W_{12} \end{bmatrix} \quad (4.15)$$

Figure 4.7 and Figure 4.8 show the simulations that compare Controller Q1 and Controller Q3. According to Figure 4.7 Controller Q3 requires faster actuator response when compared to Controller Q1. However, according to Figure 4.8b the unwanted longitudinal acceleration is greatly reduced. This is expected because high penalty is put on the acceleration state of the model used in the MPC.

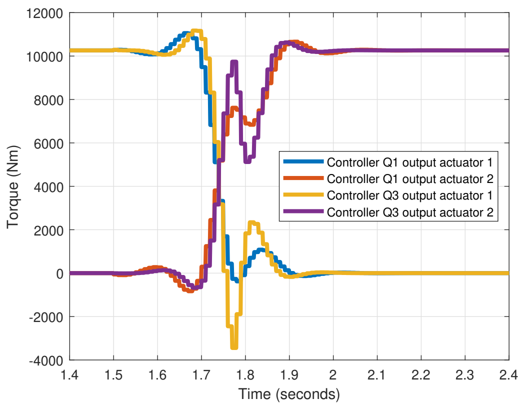

Figure 4.7: Actuator torques for Controller Q1 and Controller Q3.

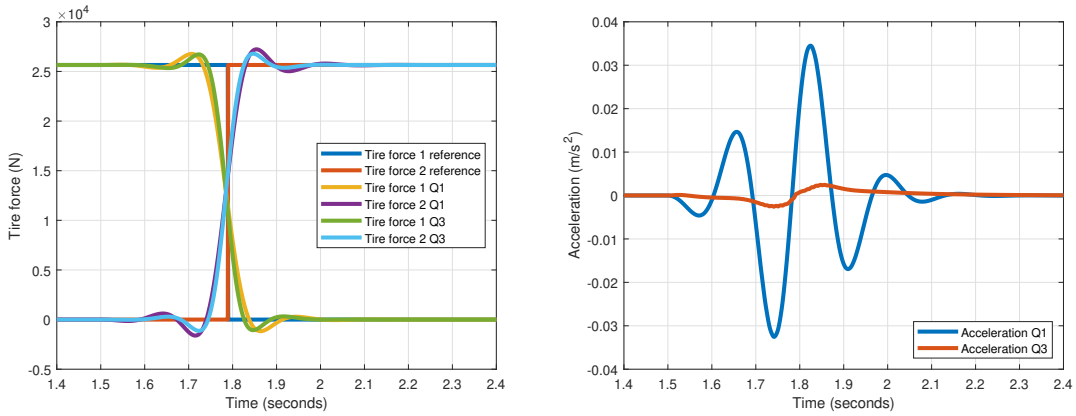

(a) Tire forces. **(b)** Acceleration.

Figure 4.8: Simulation for Controller Q1 and Controller Q3.

In the design of the fourth controller that is tested, costs are added to the derivatives of the actuator torques. This is to limit the stress on the motors and also to not require unrealistic torque variations from the electric motors. Looking back at the cost function in Equation 4.7, the controller output part of the cost function is changed as shown in Equation 4.16.

$$u(k) = \begin{bmatrix} \tau_1(k) \\ \tau_2(k) \\ \tau_{1der}(k) \\ \tau_{2der}(k) \end{bmatrix} \tag{4.16}$$

$\tau_{1der}(k)$ and $\tau_{2der}(k)$ are the discrete approximations of the derivatives of $\tau_1(k)$ and $\tau_2(k)$ respectively. The derivatives are approximately calculated using Equations 4.17 and 4.18.

$$\tau_{1der}(k) = \frac{\tau_1(k) - \tau_1(k-1)}{T} \tag{4.17}$$

$$\tau_{2der}(k) = \frac{\tau_2(k) - \tau_2(k-1)}{T} \tag{4.18}$$

The cost matrix of the inputs are modified to include the derivatives as shown in Equation 4.19.

$$R_2 = \begin{bmatrix} W_{R1} & 0 & 0 & 0 \\ 0 & W_{R2} & 0 & 0 \\ 0 & 0 & W_{R3} & 0 \\ 0 & 0 & 0 & W_{R4} \end{bmatrix} \tag{4.19}$$

Figure 4.9 and Figure 4.10 show the simulations that compare Controller Q3 and Controller Q3 R2. The weights of Controller Q3 are adjusted for tracking reference tire forces well during switching with low longitudinal acceleration. The weights of Q3 R2 also punish the derivative of actuator torque so that the torque request does not change very fast. Figure 4.9 shows that Controller Q3 R2 works as intended and decreases actuator oscillations. However, Figure 4.10 shows that the tire force

response is a little slower and the longitudinal acceleration oscillations increase for Controller Q3 R2. Thus, there is some degradation in the switching performance for Controller Q3 R2. This is expected since the requested actuator performance is more limited for this controller.

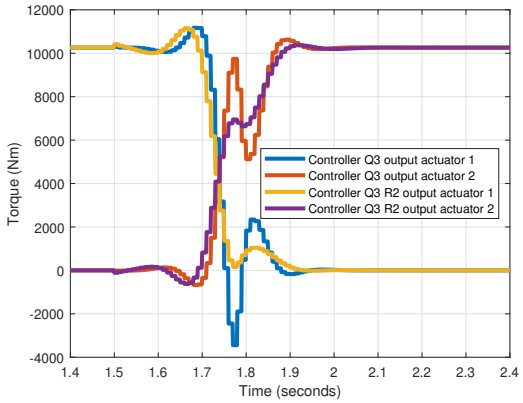

Figure 4.9: Actuator torques for Controller Q3 and Controller Q3 R2.

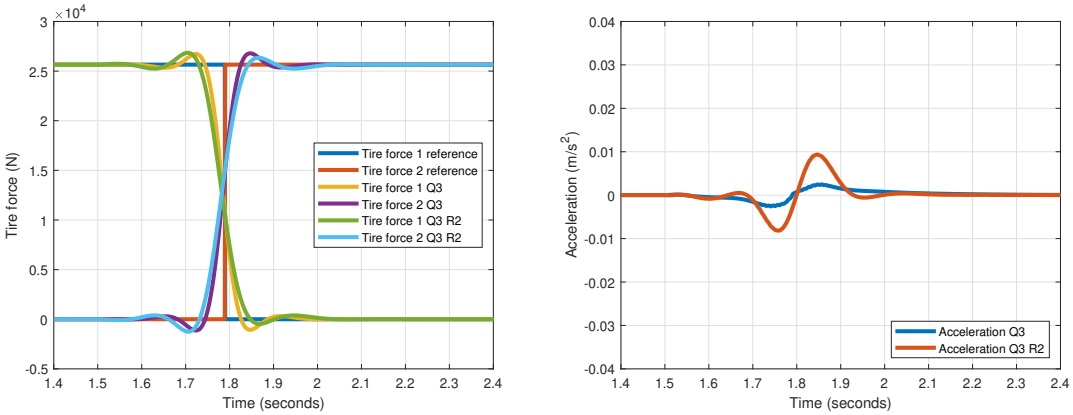

(a) Tire forces. **(b)** Acceleration.

Figure 4.10: Simulation for Controller Q3 and Controller Q3 R2.

4.2 Estimation Using the Cubature Kalman Filter

The Cubature Kalman filter is used in this thesis for parameter and state estimation. The MPC requires knowledge of all of the states to solve the optimization problem. Another issue is that the tire parameters of the vehicle are not known in general. Therefore, the tire stiffnesses of the front and rear tires are estimated as well. The Cubature Kalman filter is a nonlinear filter that approximates the nonlinearities using sigma points. It is a specific version of the Unscented Kalman filter. Since the Cubature Kalman filter is able to estimate nonlinear systems it is possible to

estimate the tire stiffnesses by adding them as states to the state equations. It is possible to use other filters for nonlinear systems such as the extended Kalman filter and the particle filter. The Cubature Kalman filter is chosen because it is better at approximating the probability distribution of a nonlinear function compared to the extended Kalman filter [21]. The disadvantage of the Cubature Kalman filter compared to the extended Kalman filter is that the computational load is higher. However, the computational load is not as high as the particle filter. The Cubature Kalman filter algorithm is described in the next subsection and the application of the filter to the longitudinal vehicle model is described in the subsection after.

4.2.1 The Cubature Kalman Filter Algorithm

The Cubature Kalman filter is a nonlinear filter but it is similar to the standard linear Kalman filter in that a Gaussian density is assumed and it consists of the prediction and update steps. The algorithm is outlined here for one prediction and one update step. As with the standard Kalman filter an initial state estimate, $\hat{\mathbf{x}}_{k-1|k-1}$, and initial covariance matrix, $\mathbf{P}_{k-1|k-1}$ at time k-1 is necessary to estimate the state at time k, $\hat{\mathbf{x}}_{k|k}$, using measurements, $\mathbf{y}_k$. Equations 4.20 and 4.21 show the creation of the sigma points. The length of state vector $\mathbf{x}$ is n. It should be noted that $\left(\mathbf{P}^{1/2}_{k-1|k-1}\right)_i$ is the i'th column of $\left(\mathbf{P}^{1/2}_{k-1|k-1}\right)$. Equations 4.22 and 4.23 show the predictions of the states and covariance respectively. The model of the system is denoted with $\mathbf{f}$ in the equations. The process noise covariance matrix is $\mathbf{Q}$ like in the standard linear Kalman filter [21].

$$\mathbf{X}^{(i)}_{k-1} = \hat{\mathbf{x}}_{k-1|k-1} + \sqrt{n}\left(\mathbf{P}^{1/2}_{k-1|k-1}\right)_i, i = 1, 2..., n \tag{4.20}$$

$$\mathbf{X}^{(i)}_{k-1} = \hat{\mathbf{x}}_{k-1|k-1} - \sqrt{n}\left(\mathbf{P}^{1/2}_{k-1|k-1}\right)_i, i = 1, 2..., n \tag{4.21}$$

$$\hat{\mathbf{x}}_{k|k-1} \approx \frac{1}{2n}\sum_{i=1}^{2n}\mathbf{f}(\mathbf{X}^{(i)}_{k-1}) \tag{4.22}$$

$$\mathbf{P}_{k|k-1} \approx \mathbf{Q}_{k-1} + \frac{1}{2n}\sum_{i=1}^{2n}(\mathbf{f}(\mathbf{X}^{(i)}_{k-1}) - \hat{\mathbf{x}}_{k|k-1})(\mathbf{f}(\mathbf{X}^{(i)}_{k-1}) - \hat{\mathbf{x}}_{k|k-1})^T \tag{4.23}$$

After the prediction step in Equations 4.20-4.23 of the Cubature Kalman filter, the update step of the filter is executed. The new sigma points are calculated using Equations 4.24 and 4.25.

$$\mathbf{X}^{(i)}_{k} = \hat{\mathbf{x}}_{k|k-1} + \sqrt{n}\left(\mathbf{P}^{1/2}_{k|k-1}\right)_i, i = 1, 2..., n \tag{4.24}$$

$$\mathbf{X}^{(i)}_{k} = \hat{\mathbf{x}}_{k|k-1} - \sqrt{n}\left(\mathbf{P}^{1/2}_{k|k-1}\right)_i, i = 1, 2..., n \tag{4.25}$$

The desired moments for use in the update step are calculated using Equations 4.26-4.28. The measurement model of the system is denoted with $\mathbf{h}$ in the equations. The measurement noise covariance matrix is $\mathbf{R}$ like in the standard linear Kalman filter.

$$\hat{\mathbf{y}}_{k|k-1} \approx \frac{1}{2n}\sum_{i=1}^{2n}\mathbf{h}(\mathbf{X}^{(i)}_{k}) \tag{4.26}$$

$$\mathbf{P}_{xyk} \approx \frac{1}{2n}\sum_{i=1}^{2n}(\mathbf{X}_k^{(i)} - \hat{\mathbf{x}}_{k|k-1})(\mathbf{h}(\mathbf{X}_k^{(i)}) - \hat{\mathbf{y}}_{k|k-1})^T \tag{4.27}$$

$$\mathbf{S}_k \approx \mathbf{R}_k + \frac{1}{2n}\sum_{i=1}^{2n}(\mathbf{h}(\mathbf{X}_k^{(i)}) - \hat{\mathbf{y}}_{k|k-1})(\mathbf{h}(\mathbf{X}_k^{(i)}) - \hat{\mathbf{y}}_{k|k-1})^T \tag{4.28}$$

The filter gain $\mathbf{K}_k$ is calculated in Equation 4.29.

$$\mathbf{K}_k = \mathbf{P}_{xyk}\mathbf{S}_k^{-1} \tag{4.29}$$

The state and covariance estimates are calculated in Equations 4.30 and 4.31.

$$\hat{\mathbf{x}}_{k|k} = \hat{\mathbf{x}}_{k|k-1} + \mathbf{K}_k(\mathbf{y}_k - \hat{\mathbf{y}}_{k|k-1}) \tag{4.30}$$

$$\mathbf{P}_{k|k} = \mathbf{P}_{k|k-1} - \mathbf{K}_k\mathbf{S}_k\mathbf{K}_k^T \tag{4.31}$$

Equations 4.20-4.31 must be applied at every time step to calculate the new state estimates and their approximate covariance matrix.

4.2.2 Application of the Cubature Kalman Filter to the Longitudinal Vehicle Model

The Cubature Kalman Filter is applied to the longitudinal vehicle model for state and parameter estimation. The tire stiffnesses are estimated by adding them as states to the state equations. The tire stiffness states are considered to be constant and vary as a random walk process. The modified version of the linear state-space longitudinal vehicle model introduced earlier is shown in Equation 4.32.

$$\begin{bmatrix} \dot{v}_{tr} \\ \dot{\omega}_{m1} \\ \dot{\theta}_{s1} \\ \dot{\omega}_{t1} \\ \dot{\omega}_{m2} \\ \dot{\theta}_{s2} \\ \dot{\omega}_{t2} \\ \dot{C}_{x1} \\ \dot{C}_{x2} \end{bmatrix} = \begin{bmatrix} \frac{-C_{x1}-C_{x2}}{m_{tr}v_{trss}} \cdot v_{tr} + \frac{C_{x1}R}{m_{tr}v_{trss}} \cdot \omega_{t1} + \frac{C_{x2}R}{m_{tr}v_{trss}} \cdot \omega_{t2} - g \cdot sin(\theta) \\ \frac{-d_{s1}}{J_{m1}} \cdot \omega_{m1} + \frac{-c_{s1}}{J_{m1}} \cdot \theta_{s1} + \frac{d_{s1}}{J_{m1}} \cdot \omega_{t1} + \frac{1}{J_{m1}}\tau_1 \\ \omega_{m1} - \omega_{t1} \\ \frac{C_{x1}R}{J_{t1}v_{trss}}v_{tr} + \frac{d_{s1}}{J_{t1}} \cdot \omega_{m1} + \frac{c_{s1}}{J_{t1}} \cdot \theta_{s1} + \frac{-d_{s1}v_{trss}-C_{x1}R^2}{J_{t1}v_{trss}} \cdot \omega_{t1} \\ \frac{-d_{s2}}{J_{m2}} \cdot \omega_{m2} + \frac{-c_{s2}}{J_{m2}} \cdot \theta_{s2} + \frac{d_{s2}}{J_{m2}} \cdot \omega_{t2} + \frac{1}{J_{m2}} \cdot \tau_2 \\ \omega_{m2} - \omega_{t2} \\ \frac{C_{x2}R}{J_{t2}v_{trss}}v_{tr} + \frac{d_{s2}}{J_{t2}} \cdot \omega_{m2} + \frac{c_{s2}}{J_{t2}} \cdot \theta_{s2} + \frac{-d_{s2}v_{trss}-C_{x2}R^2}{J_{t2}v_{trss}} \cdot \omega_{t2} \\ 0 \\ 0 \end{bmatrix} \tag{4.32}$$

For this model some of the equations have multiplication of states with each other. Therefore, the model is nonlinear. With correct measurements and tuning it is possible to estimate both the states and tire stiffnesses. If both the states and tire stiffnesses are estimated correctly the tire force can also be estimated using the tire model introduced previously. The block diagram of the application of the Cubature Kalman filter to the longitudinal vehicle model is shown in Figure 4.11.

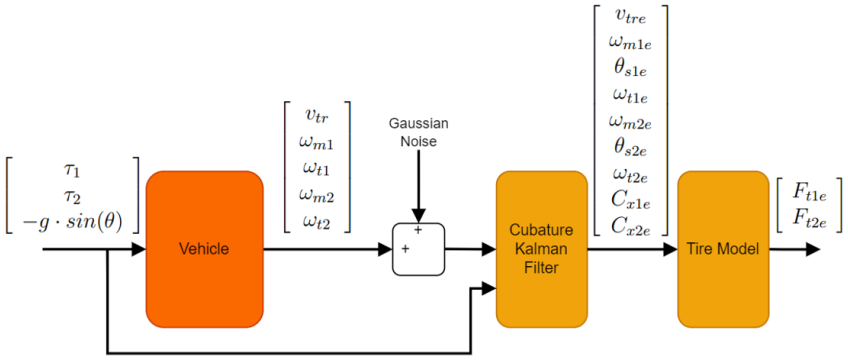

Figure 4.11: Cubature Kalman filter block diagram applied to longitudinal vehicle model.

The inputs to the vehicle shown in Figure 4.11 are as shown in Equation 2.8. These inputs are also inputs to the Cubature Kalman filter. This means that the road slope, θ is assumed to be known or estimated in another algorithm. The measurements from the real vehicle are shown in Equations 4.33.

$$y_{meas} = \begin{bmatrix} v_{tr} \\ \omega_{m1} \\ \omega_{t1} \\ \omega_{m2} \\ \omega_{t2} \end{bmatrix} \tag{4.33}$$

For the estimation process to be more realistic Gaussian noise is added to the measurements from the vehicle. The estimated states shown in the figure are also shown in Equation 4.34. It should be noted that the front and rear tire stiffnesses C_{x1e} and C_{x2e} are estimated as states using the Cubature Kalman filter. These tire stiffness estimates and vehicle state estimates are used in the tire model shown in Figure 4.11 to estimate the tire forces. The estimated front and rear tire forces are F_{t1e} and F_{t2e} respectively.

$$x_{est} = \begin{bmatrix} v_{tre} \\ \omega_{m1e} \\ \theta_{s1e} \\ \omega_{t1e} \\ \omega_{m2e} \\ \theta_{s2e} \\ \omega_{t2e} \\ C_{x1e} \\ C_{x2e} \end{bmatrix} \tag{4.34}$$

The tire forces and their estimates calculated by the filter developed in this section are shown later on in this chapter in Figure 4.19a and Figure 4.21a.

4.3 Switching Between Two Controller with Assistance of Model Predictive Controller

In Chapter 3, it was shown under certain conditions it is possible to linearly interpolate between controllers and get good results during switching. However, it was also shown that if the control system that is being switched to has considerably different dynamics than the online control system, the performance of the simple linear interpolation switching deteriorates. MPC can be used to take into account the future response of the system, the actuator and state constraints and any delays in the actuators. Therefore, MPC is a promising method for switching between two different control systems with considerably different dynamics. In this section, MPC is used to switch between two different controllers. The two axle longitudinal vehicle model will be used as the test system. Although the dynamics is not very different between the two control systems, the two axles have different dynamics mainly because of the different tire characteristics on the front and rear axles.

The general block diagram form of the MPC assisted switching system is shown in Figure 4.12. There is an online controller that is controlling the real vehicle. In this case the real vehicle is following a reference velocity. There is an offline controller that will be switched to. It is assumed that the time of switching is known. The offline controller is initially controlling a model of the real vehicle and trying to make the model follow the reference velocity. The reason for this is achieve a warm start during the switch to the offline controller. There is an MPC that will assist in the switching process to make the switch happen smoothly. The goal of the MPC is to change the tire forces requested by the online controller to the offline controller. The cost function of the MPC can be adjusted to make the process follow what is important for the designer. Furthermore, it can take into account any differences between the actuators in System 1 and System 2.

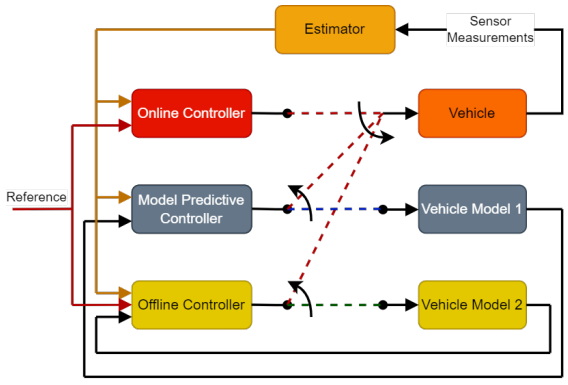

Figure 4.12: General block diagram of MPC assisted switching.

The details of the MPC assisted switching process is shown in Figure 4.13. This block diagram shows the signals in more detail. It can be seen that the tire stiffnesses are estimated by the estimator using measurements from the real system. The tire stiffness estimates are used to update the tire stiffnesses of the two vehicle

models controlled by the MPC and offline controller. Furthermore, the tire stiffness estimates are used to update the vehicle model used in the MPC for prediction purposes during the optimization. The figure also shows that the tire forces of the offline model and the online model are inputs to the MPC. This is because the goal of the MPC is to switch the tire forces from the tire forces of the online controller to the offline controller. This means that the estimator must estimate the tire forces on top of the vehicle states and tire stiffness. The MPC assisted switching is tested first with the real vehicle and the vehicle models having the same 7 state format shown in Equations 2.4-2.8. Then the VTM model is used to test MPC assisted switching for robustness. Testing with the VTM model is a relatively realistic test.

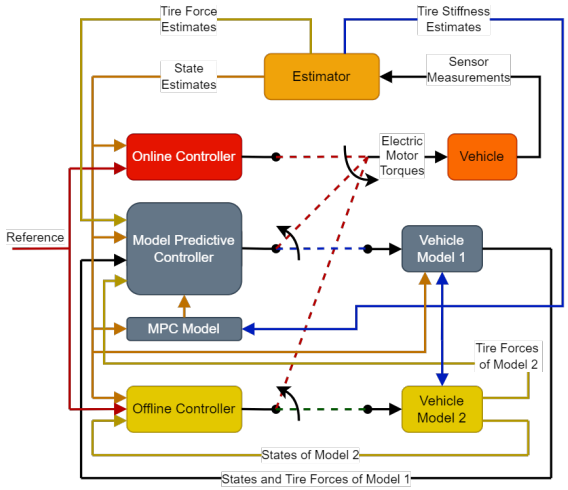

Figure 4.13: General block diagram of MPC assisted switching.

4.3.1 MPC Switching Where System Models are the Same as the Real System

In this subsection the real system and the system models are the same 7 state model shown in Equations 2.4-2.8. It should be noted that although the state-space equations are the same, the tire stiffness of the real vehicle is unknown. For this reason, the estimator estimates the tire stiffness of the real vehicle and the tire stiffnesses of the other three models are updated with this information. The switching takes 4 stages which are explained in detail now. The torque inputs to the real vehicle during all four stages is shown in Figure 4.14. For this simulation Stage 1 is between 4 and 4.5 seconds, Stage 2 is between 4.5 and 5 seconds, Stage 3 is between 5 and 6 seconds and Stage 4 is after 6 seconds into the simulation.

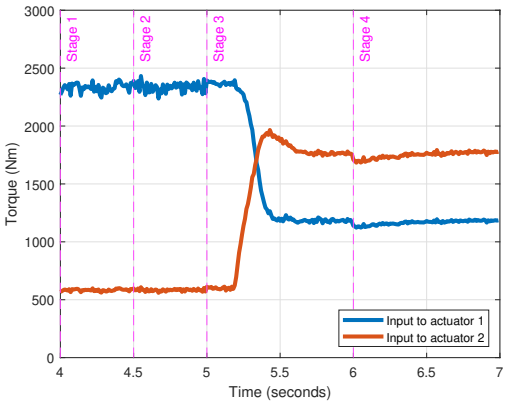

Figure 4.14: Actuator torques for MPC assisted switching during 4 stages of switching.

Block diagram of Stage 1 is shown in Figure 4.15a where the online controller is controlling the real vehicle and the actuator torques are shown in 4.15b. During Stage 1 the offline controller is connected to its own vehicle model.

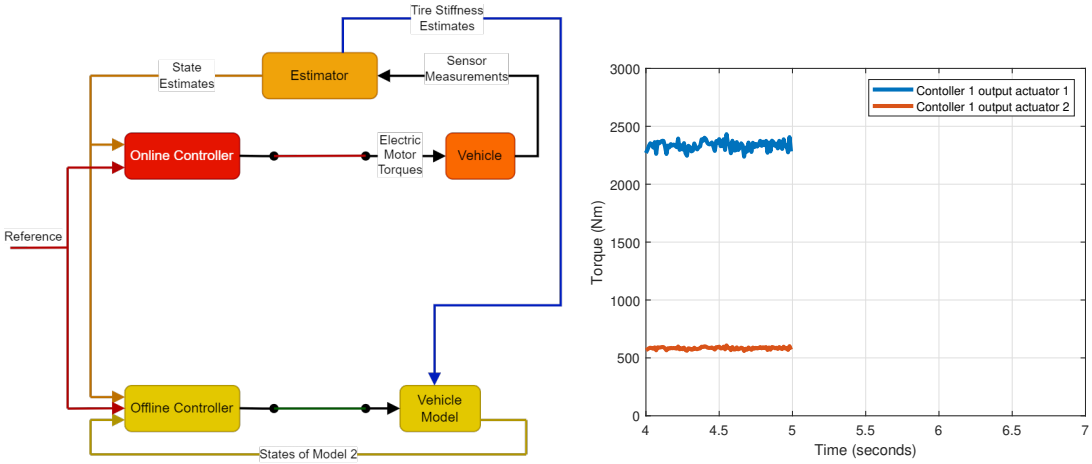

(a) Block diagram of Stage 1.

(b) Actuator torques of Stage 1.

Figure 4.15: MPC assisted switching Stage 1.

Stage 2 is shown with the block diagram in Figure 4.16a. In this stage the MPC is initialized and starts controlling its own vehicle model in a separate loop. This is to achieve a warm start during the switch from the online controller to the MPC. The vehicle model is initialized using the state estimates and tire stiffness estimates from the real vehicle. The MPC requires initial and final reference tire forces to switch between. The initial reference tire forces are obtained from the tire force estimates from the real vehicle. The final reference tire forces are obtained from the tire forces in the model controlled by the offline controller that will finally be switched to. Figure 4.16b shows the actuator torques reaching a steady state from 4.5 to 5 seconds. At 5 seconds the MPC is ready to be connected to the real vehicle.

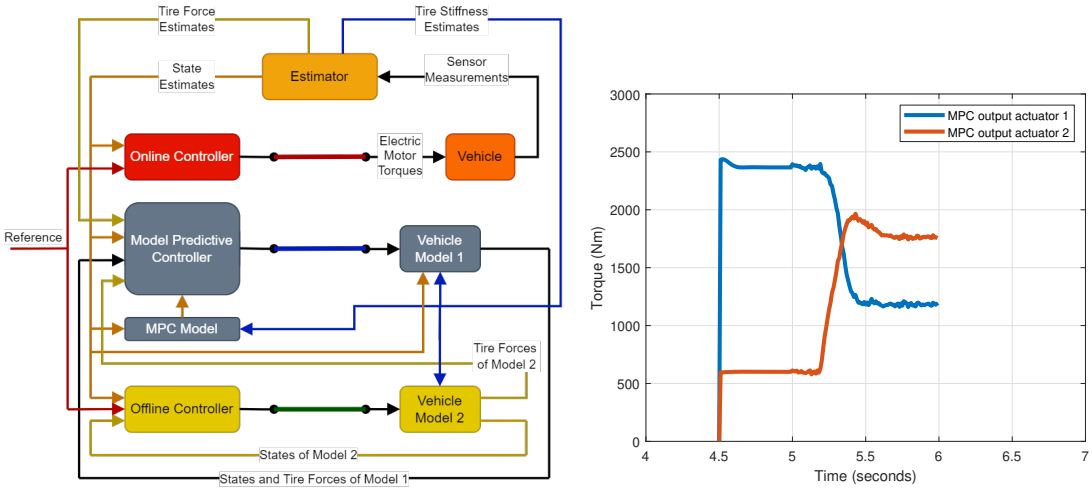

(a) Block diagram of Stage 2. **(b)** Actuator torques of Stage 2.

Figure 4.16: MPC assisted switching Stage 2.

Figure 4.17a shows Stage 3 with a block diagram. During Stage 3 the MPC takes over controlling the real vehicle. Switching the tire forces from the tire forces produced by online controller to the tire forces produced by offline controller is executed. It should be noted that both of these tire forces are estimates. Tire forces of the real vehicle cannot be measured and therefore must be estimated. Furthermore, the tire forces that will be determined by the offline controller after it is connected is also not known because the vehicle model is not exactly the same as the real vehicle. The torque variation during the switching process is shown in Figure 4.17b.

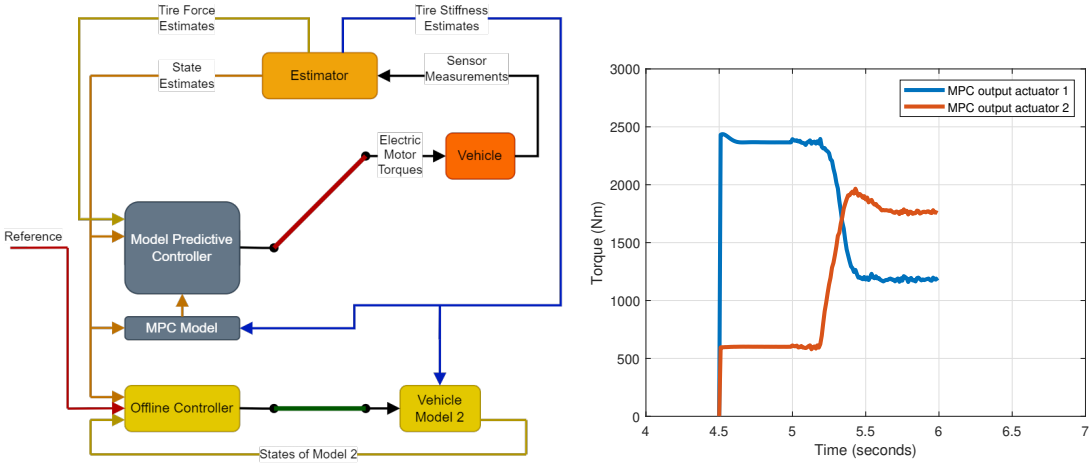

(a) Block diagram of Stage 3. **(b)** Actuator torques of Stage 3.

Figure 4.17: MPC assisted switching Stage 3.

Stage 4 is shown with a block diagram in Figure 4.18a. This stage is the final stage and the final controller is connected to the real vehicle. Now, the new controller both controls the torques going into the real vehicle and also starts using the measurements from the real vehicle. It is not connected to the offline vehicle model

anymore. The electric motor torque is shown in Figure 4.18b for Stage 4 shows a small bump when the switch occurs.

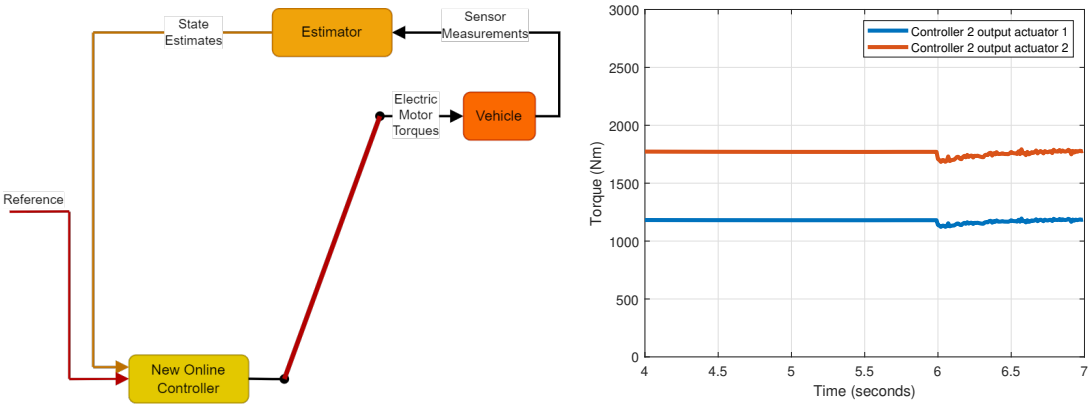

(a) Block diagram of Stage 4. **(b)** Actuator torques of Stage 4.

Figure 4.18: MPC assisted switching Stage 4.

Tire forces and their estimates are shown in Figure 4.19a.The noisy estimates are on top of the actual tire forces so they are not visible. This shows that the tire force estimates are quite accurate. The velocity plot shown in Figure 4.19b shows that the velocity increases slightly during the switching process. This occurs because the controller currently used is just trying to switch the forces by minimizing a cost function and the cost function does not take into account velocity. It should be noted that it is possible to add the velocity into the cost function to keep it constant. Since the velocity has increased slightly during the switch the final controller starts decreasing the velocity when Stage 4 begins. This is the reason of the small bump in decreasing electric motor torques that is observed in Figure 4.19a at the beginning of Stage 4.

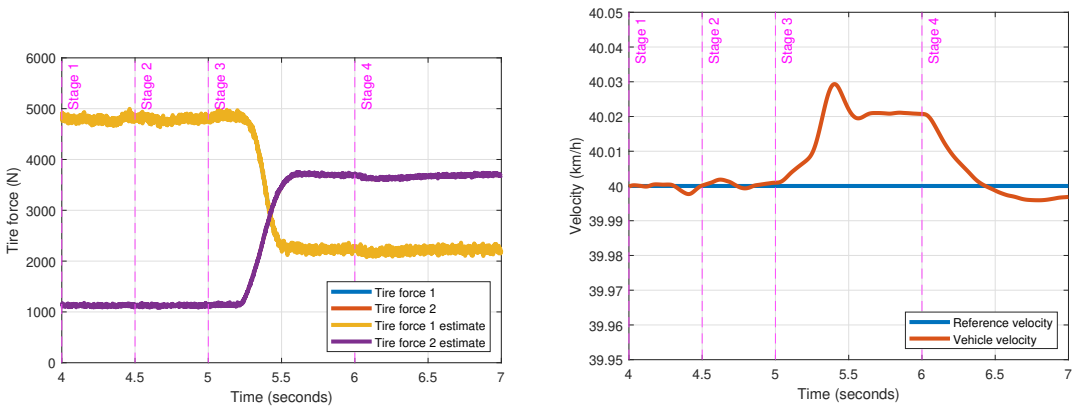

(a) Tire forces and estimates. **(b)** Velocity.

Figure 4.19: Tire forces and velocity for MPC assisted switching during 4 stages of switching.

4.3.2 MPC Switching Where System Models are the 7 State Model and the Real System is the VTM Model

The same simulation is conducted as in the previous section, but this time the real vehicle is the VTM model. The electric motor torques for this simulation are shown in Figure 4.20. The switching process goes through the same 4 stages. The only difference is that Stage 3 lasts shorter and Stage 4 starts at 5.7 seconds. It was observed that the longer Stage 3 continues, the more the vehicle velocity deviates from the reference velocity. Therefore, exiting Stage 3 faster results in a smaller bump in electric motor torques.

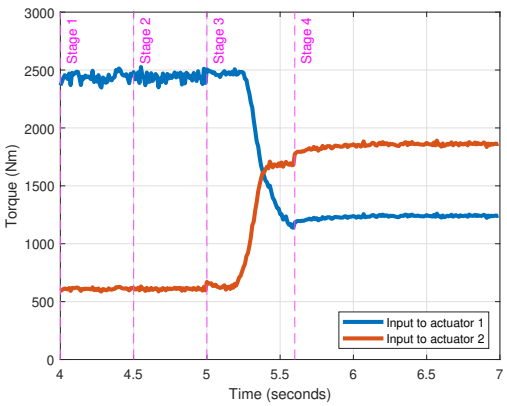

Figure 4.20: Actuator torques for MPC assisted switching during 4 stages of switching.

Figure 4.21a shows the tire forces and tire force estimates during the full simulation. It can be seen that the tire force estimates are better before the switch when compared with after the switch. The possible reason for this is that the tire stiffness is being estimated before the switch and the tire moves to a different operating point after the switch. Therefore, the tire model's accuracy decreases after the switch. Tire force modeling is a very complicated topic where very detailed models are used that only work under certain conditions. The accuracy of the tire force estimate is acceptable since a simple linear tire model with unknown stiffness was used in the estimation. Figure 4.21b shows that the velocity of the vehicle deviates very slightly from the reference value and moves towards the correct value during Stage 4.

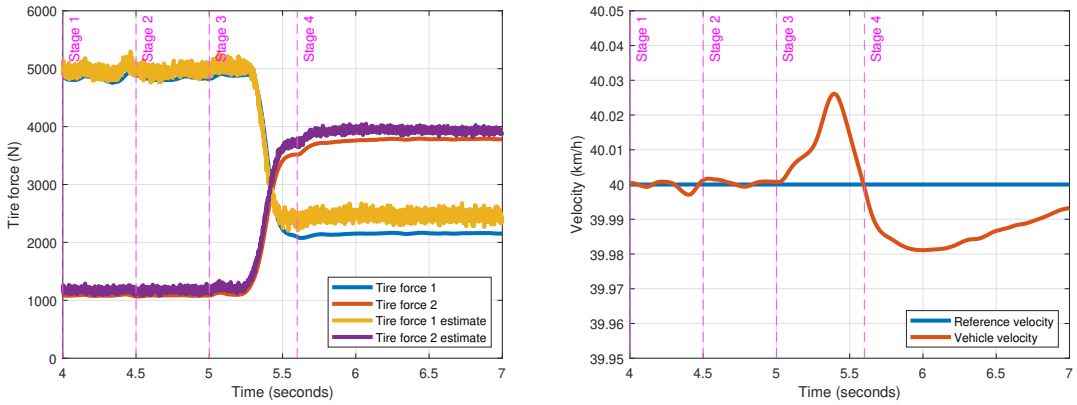

(a) Tire forces and estimates. **(b)** Velocity.

Figure 4.21: Tire forces and velocity for MPC assisted switching during 4 stages of switching.

5

Controller Switching Using Sigmoid Functions

In this chapter a case study of switching between a CA control algorithm and a rule based algorithm is analyzed.

5.1 Using a Sigmoid Function for Switching

The general switching control system that is analyzed in this chapter is shown in Figure 5.1. An important difference between the control switching performed in this chapter compared to previous chapters is that the outside controller in the loop is the same for both of the controllers. Here, the driver, which is the driver model found in VTM is trying to keep the velocity of the vehicle constant. The driver outputs a reference force for the total vehicle. As in the previous simulations the vehicle is traveling straight and the lateral dynamics of the vehicle are not analyzed. The vehicle is traveling downhill where the slope of the road is 5 degrees. The driver is braking the vehicle to maintain constant velocity. Initially a CA determines how to distribute the driver force request. Then a switch to a rule-based controller is performed. The CA distributes the torques on the front and rear tires according to the efficiency of the electric motors using an optimization algorithm. The rule-based algorithm divides the torques between the front and the rear depending on the normal forces on the front and rear axles. The goal is to analyze switching performance from an optimization based algorithm that minimizes energy consumption to a simple rule based allocator.

The CA optimizes by calculating the proportion the brake and electric motors are used for highest efficiency. However, for this downhill simulation where the electric motors provide enough torque to keep the speed constant by regenerative torque, the CA chooses to only use the electric motors and does not use the mechanical brakes. On the other hand, the rule based algorithm is assumed to only have access to using the mechanical brakes to control the speed. There is a significant difference in the response time of the two actuators. The electric motors respond almost instantaneously and is modeled with the transfer function is Equation 5.1 where $\tau_e = 0.001$.

$$T_e(s) = \frac{1}{\tau_e s + 1} \tag{5.1}$$

The mechanical brakes respond slower and are modeled with the transfer function

in Equations 5.2. The brake model has a dead time component where $\theta_b = 0.02$ and a first order delay component where $\tau_b = 0.22$.

$$T_b(s) = \frac{e^{-\theta_b s}}{\tau_b s + 1} \tag{5.2}$$

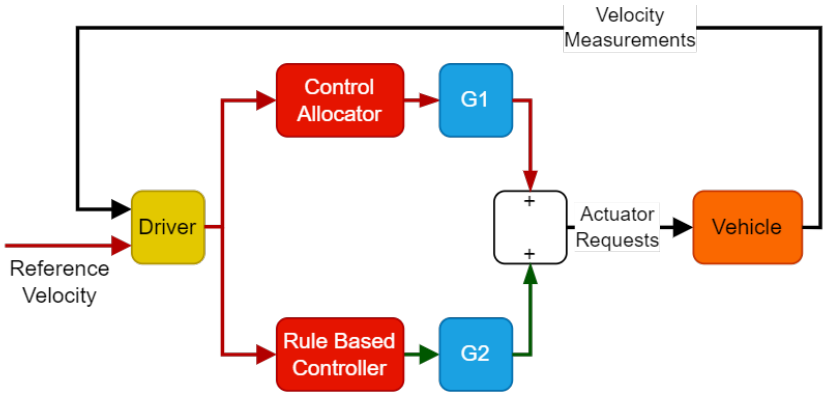

Figure 5.1: Block Diagram for switching between CA and rule based method using sigmoid function.

Sigmoid functions are used for the gains G1 and G2 shown in Figure 5.1 for switching purposes. Gain G1 is decreased from 1 to 0 and G2 is increased from 0 to 1 during switching using sigmoid functions. The G2 function is a sigmoid function as shown in Equation 5.3 where K_s determines slope of the sigmoid and t_d determines the time that the switch occurs. The plot of the sigmoid in time is shown in Figure 5.2 where the blue line is the plot of Equation 5.3 for $K_s = 20$. The G1 function is found by subtracting G2 from 1. The plot of G1 in time is also shown in Figure 5.2 but with an orange line.

$$G2(t) = \frac{1}{1 + e^{-K_s(t-t_d)}} \tag{5.3}$$

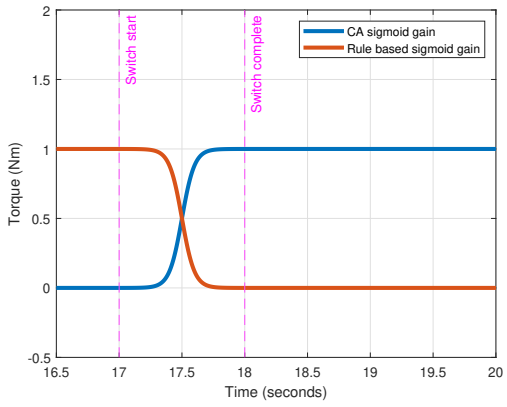

Figure 5.2: Sigmoid function based gain variation for switching.

5.2 Control Allocation Controller Failure Scenario

Switching using the method developed in the previous section is tested for a CA failure scenario. It is possible for a CA to not have feasible solutions to the optimization problem and output unexpected results. This possibility must be taken into account in the design of the control system. In this section, a CA failure is simulated. During the first 17 seconds of the simulation the vehicle is traveling downhill with a constant velocity and the CA is braking with the electric motors by dividing the torque between the front and rear electric motors for optimal energy regeneration. At 17 seconds into the simulation, the CA fails to find a feasible solution and starts outputting 0 torque requests for the front and rear tires as shown in Figure 5.3a and Figure 5.3b, respectively. The switching process described in the previous section is started when the failure occurs. At 17 seconds the rule based algorithm is outputting a front and rear tire torque as well as shown in Figures 5.3a and 5.3b, respectively. These figures show the request for the front and rear tire torques to switch from the CA request to the rule based request between 17 seconds and 18 seconds in the simulation using sigmoid functions. It should be noted that these are the requests and not the actual torques at the tires. Since the actuators take time to respond, the actual torques occur with a certain amount of delay when compared with the requests. The actuator requests and their respective outputs are shown in Figure 5.4a and Figure 5.4b.

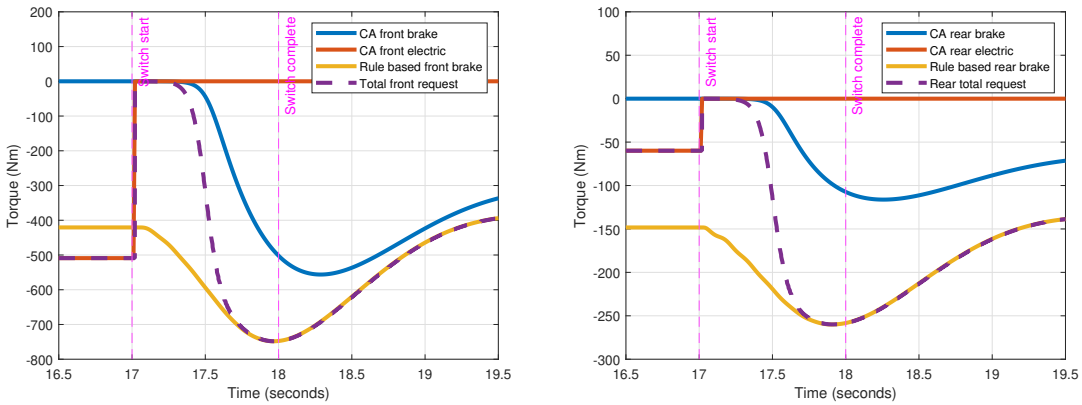

(a) Front tire. **(b)** Rear tire.

Figure 5.3: Torque requests during switching after CA failure.

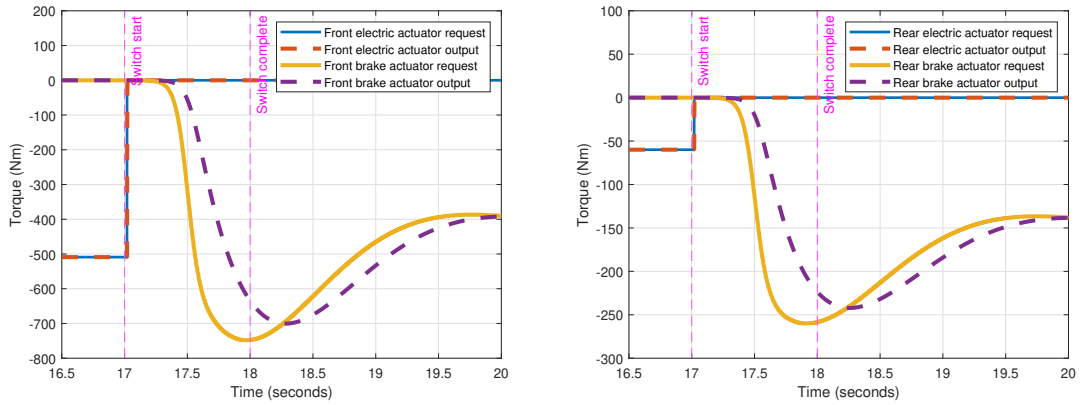

(a) Front tire. **(b)** Rear tire.

Figure 5.4: Actuator outputs during switching after CA failure.

The resulting tire torques on the front and rear tires are shown in Figure 5.5a. The corresponding vehicle velocity for these tire torques is shown in Figure 5.5b. Figure 5.5b shows that the error in velocity tracking increases after the CA failure and then goes back to the value before the failure after the switch to the rule based controller. It should be noted that there is a driver model that is simulated by a controller which responds to the increase in the error after the CA failure. Figure 5.6 shows that the braking force requested by the driver increases in the absolute sense as the vehicle speed increases. This is the reason why there are oscillations in the tire torques before the tire torques settle down to the rule based tire torque requests which were being requested previous to the CA failure.

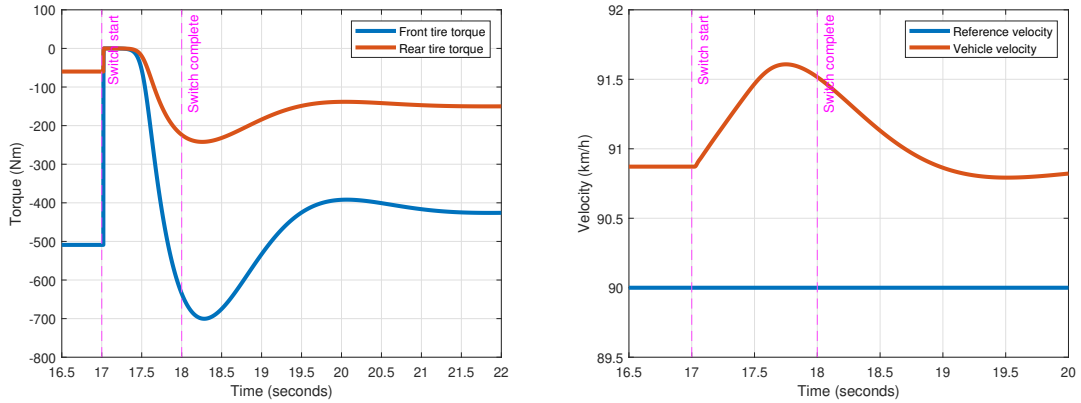

(a) Front and rear total tire torque. **(b)** Vehicle speed.

Figure 5.5: Vehicle response during switching after CA failure.

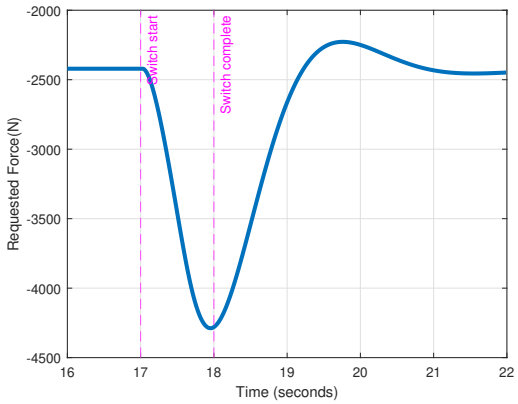

Figure 5.6: Tire force requested by driver during switching after CA failure.

5.3 Control Allocation Output Hold for Improved Switching Performance

In Section 5.2, failure in the CA produced a temporary 0 actuator request which caused an undesired response. A possible solution to this problem is to continue with the same CA output request when the failure occurs and switch to the rule based output request using the sigmoid function gains. This method is tested through simulations in this section. Figure 5.7a and 5.7b show the front and rear tire torque requests respectively. The CA fails at 17 seconds in these figures as well. However, the last value before the failure is held constant as an output for the CA. The actuator requests during the switch are less oscillatory and have smaller overshoots which suggest a better response with this method.

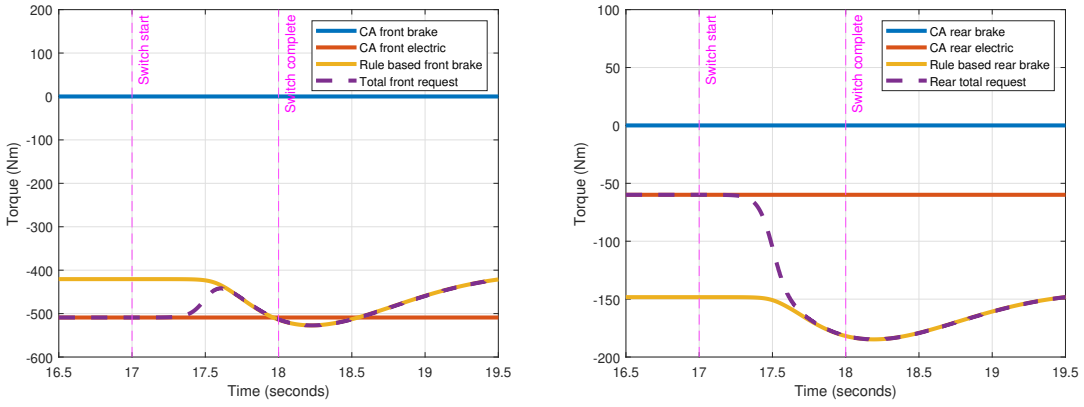

(a) Front tire. **(b)** Rear tire.

Figure 5.7: Torque requests during output hold switching after CA failure.

Figure 5.8a and Figure 5.8b show that even though the actuator torque requests resemble the sigmoid function quite closely, the actuator responses are not symmetric. This is because the brake actuator that is coming online is much slower than the

electric motor actuator that is going offline. Figure 5.8a and Figure 5.8b show that the electric motor output and the request are almost exactly tracking each other whereas the mechanical brake response is lagging the brake request. The results of the delay in the mechanical brake response can be seen in the decrease in the total tire torque shown in Figure 5.9a. This results in a slight increase in the speed of the vehicle as shown in Figure 5.9b. The increase in the vehicle velocity, in turn results in an increase of the requested driver torque to decrease the velocity as shown in Figure 5.10. The increase in vehicle speed shown in Figure 5.5b is approximately three times higher than the vehicle speed increase shown in Figure 5.9b. The increase in the requested driver torque shown in Figure 5.6 is also approximately three times higher than the increase in the requested driver torque shown in Figure 5.10. These figures show that there is a significant improvement in the performance of the switching process when the CA output is held after the CA failure occurs.

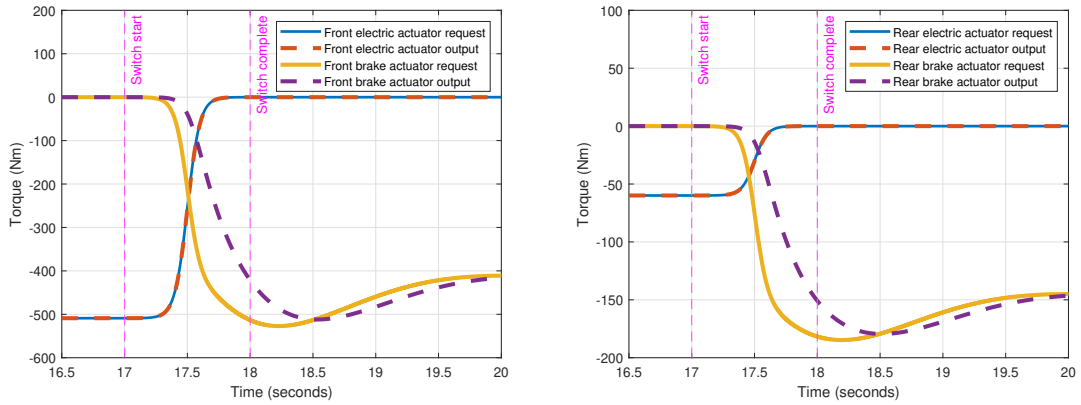

(a) Front tire. **(b)** Rear tire.

Figure 5.8: Actuator outputs during output hold switching after CA failure.

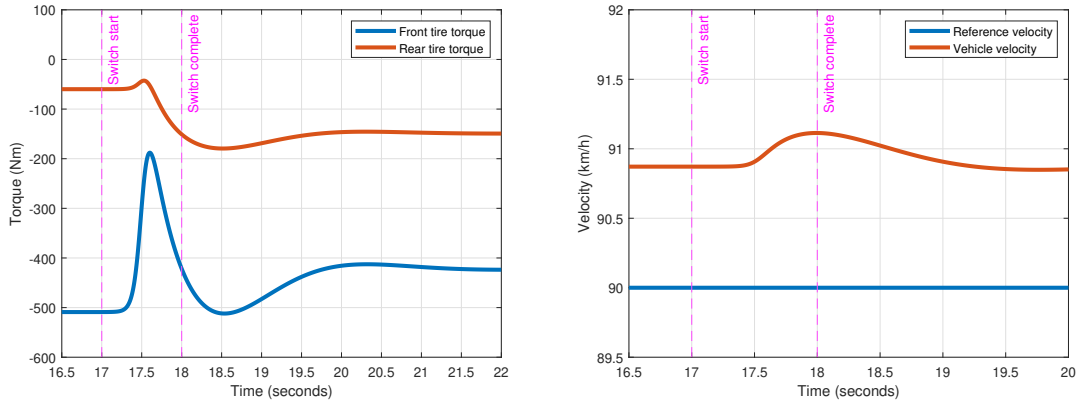

(a) Front and rear total tire torque. **(b)** Vehicle speed.

Figure 5.9: Vehicle response during output hold switching after CA failure.

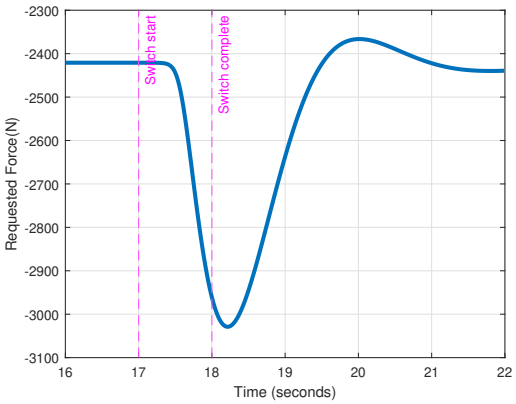

Figure 5.10: Tire force requested by driver during output hold switching after CA failure.

5.4 Shaping Switching Functions for Improved Switching Performance

The previous section showed that using symmetric sigmoid functions for switching will not produce ideal results when the actuators that are switched between do not have the same response rate. This happens when the actuators coming offline are responding at a different rate than the the actuators coming online which results in the replacement of torques being too fast or too slow. If there is good information about the actuator response times, this information can be incorporated into the switching sigmoid functions. For the example in this chapter, the electric motor responds much faster compared to the mechanical brakes. So, as the electric motors go offline, the mechanical brake torques cannot catch up. This information is incorporated into the sigmoid function by filtering the electric motor sigmoid functions by the approximate transfer function of the mechanical brakes. This results in the filtered sigmoid functions shown in Figure 5.11. The figure shows the request for the electric motors to go offline is slower than the request of the mechanical brakes to come online.

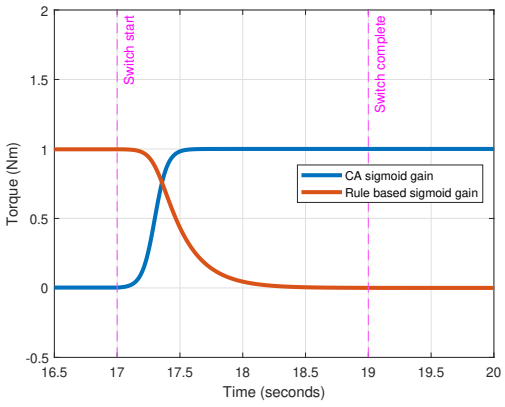

Figure 5.11: Filtered sigmoid function based gain variation for switching.

Applying the sigmoid functions shown in Figure 5.11 for the switching process results in the torque requests shown in Figures 5.12a and 5.12b. These figures show that the total request becomes quite large. However, Figures 5.13a and 5.13b show that the actuator responses during the switching process are quite symmetric. This results in the very smooth transform of the total tire torques from the CA request to the rule based controller request as shown in Figure 5.14a. Furthermore, the change in the vehicle velocity is barely visible in Figure 5.14b. The change in driver force request during the switching phase is also very small as shown in 5.15. These figures show that shaping the switching functions was successful in making the switching process very smooth.

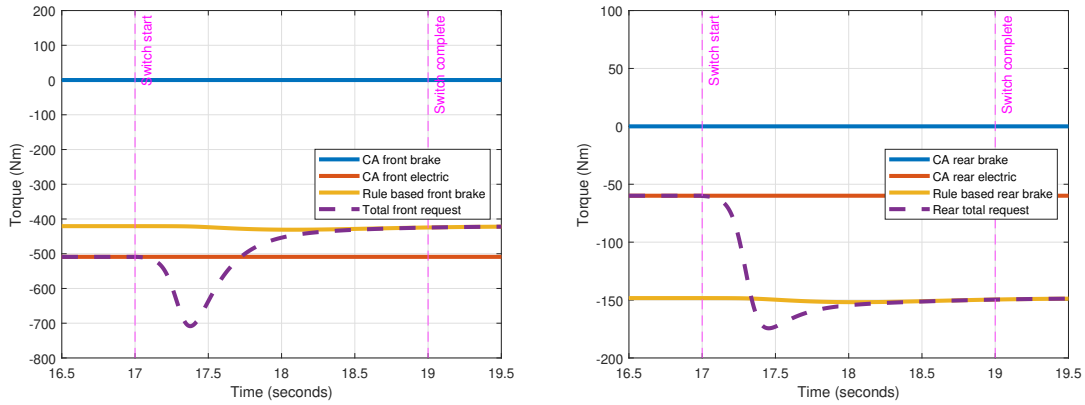

(a) Front tire. **(b)** Rear tire.

Figure 5.12: Torque requests during filtered sigmoid based switching after CA failure.

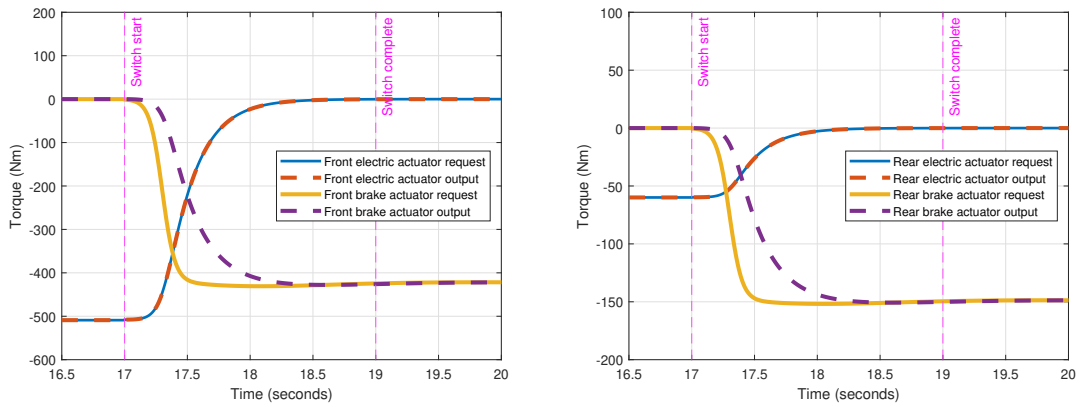

(a) Front tire. **(b)** Rear tire.

Figure 5.13: Actuator outputs during filtered sigmoid based switching after CA failure.

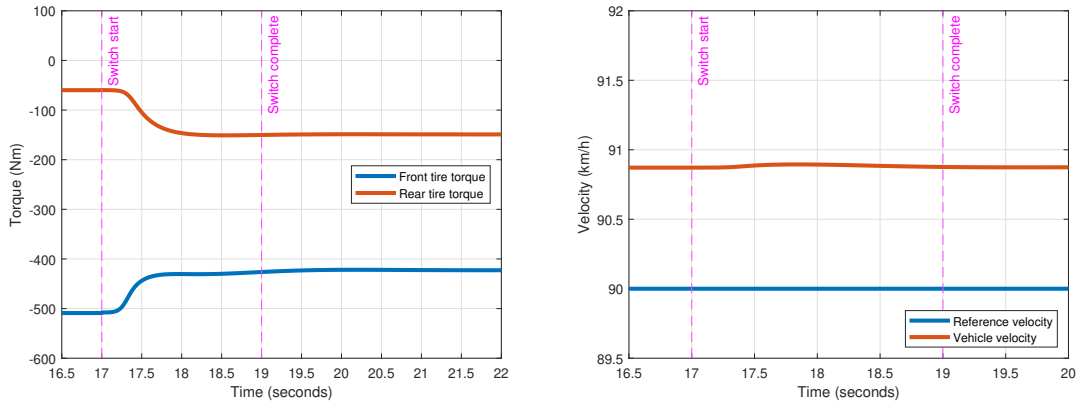

(a) Front and rear total tire torque. **(b)** Vehicle speed.

Figure 5.14: Vehicle response during filtered sigmoid based switching after CA failure.

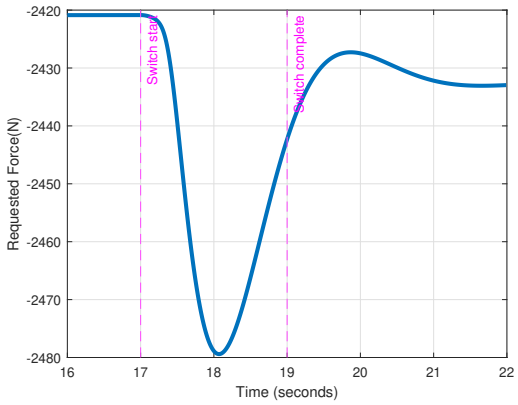

Figure 5.15: Tire force requested by driver during filtered sigmoid based switching after CA failure.

6
Conclusion

6.1 Conclusions

Possible issues in switching between different vehicle dynamics controllers used in heavy vehicles have been analyzed in this thesis. It was observed that switching between controllers that have their own dynamics (for example a PI controller) are specifically problematic since the dynamics of the controllers interact with the vehicle dynamics when the switch is made. A proposed solution is to keep the offline controller connected to a model of the real vehicle to keep the controller at a state that is close to the state it will have when it is connected to the real vehicle. This method was shown to work better than connecting a controller that was not prepared. Linear interpolation between the outputs of two controllers was shown through simulations to give an easy implementation and smooth transition between two different controllers.

Model Predictive Control (MPC) was shown to be an alternative method for switching. Several advantages of the MPC were observed. One important advantage of the MPC is observed when the timing of the switch is known. When the time of the switch is known, this time can be put into the optimization function. The MPC takes this information into account and optimizes the actuation to minimize the cost function taking the switch into account. This results in the actuation to start even before the switch time so that switching is as smooth as possible. On the other hand, an unexpected switch with a similar cost function resulted in larger oscillations in the forces. This, in turn resulted in larger acceleration disturbances to the vehicle. Another advantage of the MPC is to be able to put different weights on different variables so that the control design engineer can focus the controller for example on fast response, less actuator wear or passenger comfort. In general, MPC based switching was seen to give the control design engineer specific control into all aspects of the switching process. Even though the MPC based switching process was complex it was shown to work in a realistic simulation environment.

MPC is a very powerful tool in the switching process, yet three main disadvantages were observed. The first disadvantage is the computational load on the controller. Even though this thesis did not focus on computational load, it is well known that online MPC solvers take longer times to compute outputs compared to more traditional controllers used in vehicles. Possible consequences of this is the necessity of a more powerful processor in the vehicle compared to standard vehicles. This would

result in an increase in the price of the vehicle which is undesirable in the highly competitive market of vehicle manufacturing. Another issue of using an MPC is for the MPC to not be able to find a solution to the optimization problem in a reasonable amount of time. This is specifically true for nonlinear MPCs which were not considered in this thesis.

The second disadvantage of the MPC is that the MPC requires all the states of the vehicle to be known. Since all of the states cannot be measured, the unmeasured states must be estimated. A Cubature Kalman filter was developed and used for the estimation of the states that were not possible to measure. Since a simulation environment was used, noise was added to the measurements from the "real" system to simulate more realistic scenarios. The magnitude of the noise affected the performance of the MPC. There was a trade-off between the amount of noise allowed and the performance of the MPC. Specifically for large noise to signal ratios, there was a limit to the amount that the unwanted acceleration of the vehicle could be decreased. It should be noted that a smaller sampling time for the Kalman filter compared to the MPC was seen to give better performance in the overall system. A sampling time of 0.001 seconds for the Kalman filter and a sampling time of 0.01 seconds for the MPC was observed to achieve good performance. It should be noted that decreasing the sampling times of both the Kalman filter and the MPC improves the performance of each of them and the system overall. However, the computational cost of decreasing the sampling time of the MPC is much higher. This is because the MPC needs to predict a certain amount of time into the future to achieve good performance. However, when the sampling time is decreased the number of prediction steps in the horizon of the MPC must be increased by the same proportion to achieve the same total prediction horizon. This results in an exponential increase in the computation time for the MPC, thus limiting the sampling time of the MPC.

The third disadvantage of using an MPC is that it requires a model in the predictive optimization process. The problem with optimization using a model is that models do not fully represent reality. The effect of this was studied in two different stages. Tire properties are among the most difficult parts of the vehicle to model. In the first stage the "real" vehicle was taken as the as the vehicle model developed in this thesis. Even though a linear tire model was used, the tire stiffnesses of the front and rear tires were assumed to be unknown. Thus, a Cubature Kalman filter was used to estimate the tire stiffnesses as well as the states of the vehicle. The Kalman filter was able to estimate the tire stiffness, tire forces and vehicle states accurately even in the presence of noise. This was expected since the "real" system and the Kalman filter model were quite similar. Switching between controllers with the MPC worked well under these circumstances. In the second stage of testing model inaccuracies, the VTM model was used as the "real" system during the simulation. This simulation is more realistic since a nonlinear real system is being controlled by the MPC. However, the Kalman filter update model and the MPC prediction model are linear models. There was some deterioration in the performance of the switching process. A partial explanation of this deterioration is the inaccuracy in the tire force estimation. There are two main reasons for the inaccuracy in the tire force estimation. The first is the

very nonlinear nature of the "real" tire. The second is the sensitivity of calculation of tire slip to tire radius which is also a very difficult parameter to measure or estimate.

In the final section of the thesis a case study of switching using sigmoid functions from a CA controller to a rule based controller was analyzed. The scenario was of a truck traveling downhill while the driver was trying to keep constant velocity by braking. There were two reasons for the choice of this scenario. The first interesting part is the switching between a dynamics optimization based controller to a rule based controller. The second interesting part of this case study was the fact that the response times of the systems before and after the switch were quite different. The CA was controlling electric motors during the braking process whereas the rule based algorithm was assumed to only have access to mechanical brakes which had a much slower response rate. The problems associated with just using a sigmoid function during a CA failure were shown. Solutions to these problems were developed. It was shown that the last output of the CA can be held constant and the sigmoid functions can be used to switch from these outputs to the rule based controller. Even though this method worked reasonably well the difference between the response rates of the actuators still caused a disruption in the total tire force and vehicle velocity. The filtering of the sigmoid functions used in switching depending on the actuator response rates was tested as a solution to this disruption. The filtering of the switching sigmoid functions depending on the actuator response rates decreased the disruption during switching to negligible levels.

6.2 Future Work

The switching methods developed in this thesis were tested in a simulation environment with a realistic model developed by Volvo (VTM). However, even though the vehicle model was very detailed, the braking system model and electric motor models were relatively simple. Simulating with more detailed electric motor and mechanical braking models can give more realistic results even in the simulation environment.

The performance of the longitudinal vehicle dynamics during the switching process was analyzed in this thesis. It is well known that the lateral and longitudinal dynamics of a vehicle are coupled. Therefore, including the lateral dynamics of the vehicle in the analysis is the next step in predicting how the vehicle dynamics change during the switching process.

Real time testing of the controllers and switching methods was not implemented. Testing the real time implementation of the MPC is especially crucial because of the computational intensity of the optimization process. Therefore, real time testing of the controller on a dedicated controller is the next step in determining the viability of the MPC.

Analysis of the effects of sample time and noise of sensors was performed in this thesis. The sampling time and sensor accuracy on current truck systems is not

capable of running the algorithms developed in this thesis. The requirements on the computer system and sensors is an area that can be researched further. It should be pointed out that the next generation of computer systems and sensors that are planned to be implemented on trucks are much faster and more accurate. This trend of increasing computing power and more accurate sensors in heavy vehicles is expected to continue.

Bibliography

[1] K. Bengler, K. Dietmayer, B. Farber, M. Maurer, C. Stiller, and H. Winner, "Three decades of driver assistance systems: Review and future perspectives," *IEEE Intelligent transportation systems magazine*, vol. 6, no. 4, pp. 6–22, 2014.

[2] U. N. D. of Economic and S. Affairs, "Sustainable transport, sustainable development," in *Interagency Report, Proceedings of the Second Global Sustainable Transport Conference, Beijing, China, 14–16 October 2021*. United Nations New York, NY, USA, 2021.

[3] V. Keller, B. Lyseng, C. Wade, S. Scholtysik, M. Fowler, J. Donald, K. Palmer-Wilson, B. Robertson, P. Wild, and A. Rowe, "Electricity system and emission impact of direct and indirect electrification of heavy-duty transportation," *Energy*, vol. 172, pp. 740–751, 2019.

[4] S. Janardhanan, E. Gelso, L. Laine, M. Jonasson, and B. Jacobson, "Reviewing control allocation using quadratic programming for motion control and power coordination of battery electric vehicles," in *2022 IEEE Vehicle Power and Propulsion Conference (VPPC)*. IEEE, 2022, pp. 1–8.

[5] K. Tagesson, P. Sundstrom, L. Laine, and N. Dela, "Real-time performance of control allocation for actuator coordination in heavy vehicles," in *2009 IEEE Intelligent Vehicles Symposium*. IEEE, 2009, pp. 685–690.

[6] C. Edwards and I. Postlethwaite, "Anti-windup and bumpless-transfer schemes," *Automatica*, vol. 34, no. 2, pp. 199–210, 1998.

[7] M. Pasamontes, J. D. Álvarez, J. L. Guzmán, and M. Berenguel, "Bumpless switching in control-a comparative study," in *2010 IEEE 15th Conference on Emerging Technologies & Factory Automation (ETFA 2010)*. IEEE, 2010, pp. 1–8.

[8] M. Werling, M. Kaufmann, and L. Gröll, "Different schemes for bumpless manual/automatic transfer," in *9th Internation Workshop on Research and Education in Mechatronics, Bergamo, Italy*, 2008, pp. 129–130.

[9] D. N. Godbole and J. Lygeros, "Longitudinal control of the lead car of a platoon," *IEEE Transactions on Vehicular Technology*, vol. 43, no. 4, pp. 1125–1135, 1994.

[10] K. Zheng and J. Bentsman, "Input/output structure of the infinite horizon lq bumpless transfer and its implications for transfer operator synthesis," *International Journal of Robust and Nonlinear Control: IFAC-Affiliated Journal*, vol. 20, no. 8, pp. 923–938, 2010.

[11] I. Malloci, L. Hetel, J. Daafouz, C. Iung, and R. Bonidal, "Bumpless transfer for discrete-time switched systems," in *2009 American Control Conference*. IEEE, 2009, pp. 1078–1083.

[12] M. C. Turner and D. J. Walker, "Linear quadratic bumpless transfer," *Automatica*, vol. 36, no. 8, pp. 1089–1101, 2000.
[13] F. R. P. Safaei, J. P. Hespanha, and G. Stewart, "On controller initialization in multivariable switching systems," *Automatica*, vol. 48, no. 12, pp. 3157–3165, 2012.
[14] G. Nestlinger and M. Stolz, "Bumpless transfer for convenient lateral car control handover," *IFAC-PapersOnLine*, vol. 49, no. 15, pp. 132–138, 2016.
[15] S. Skogestad and I. Postlethwaite, *Multivariable feedback control: analysis and design*. john Wiley & sons, 2005.
[16] J. D. Boskovic and R. K. Mehra, "Multi-mode switching in flight control," in *19th DASC. 19th Digital Avionics Systems Conference. Proceedings (Cat. No. 00CH37126)*, vol. 2. IEEE, 2000, pp. 6F2–1.
[17] S. H. Cha *et al.*, "Guaranteed safe switching for switching adaptive control," 2010.
[18] A. S. Morse, "Supervisory control of families of linear set-point controllers-part i. exact matching," *IEEE transactions on Automatic Control*, vol. 41, no. 10, pp. 1413–1431, 1996.
[19] D. Liberzon and A. S. Morse, "Basic problems in stability and design of switched systems," *IEEE control systems magazine*, vol. 19, no. 5, pp. 59–70, 1999.
[20] T. Glad and L. Ljung, *Control theory*. CRC press, 2000.
[21] L. Hammarstrand, "Chalmers university of technology lecture notes, ssy345 sensor fusion and nonlinear filtering," 2022.

DEPARTMENT OF ELECTRICAL ENGINEERING
CHALMERS UNIVERSITY OF TECHNOLOGY
Gothenburg, Sweden
www.chalmers.se

CHALMERS
UNIVERSITY OF TECHNOLOGY